


Cite this: *RSC Adv.*, 2023, **13**, 10800

Received 13th February 2023  
Accepted 28th March 2023

DOI: 10.1039/d3ra00966a

rsc.li/rsc-advances

## 1. Introduction

Materials science, energy science, and information science are the three key branches of modern science and technology. Materials science is particularly important as it has been dominant since ancient times. Among the various materials reported, porous materials have attracted considerable attention. Metal–organic frameworks (MOFs) are nano-materials with different topological structures and highly ordered pores, which have been developed by the coordination of multiple organic ligands and inorganic metal ions.<sup>1–4</sup> Owing to the diversity of organic ligands and metal ions, various MOFs have been developed and attracted the attention of researchers in chemistry, materials science, and physics.<sup>5,6</sup> Compared with conventional porous materials, MOFs with increased specific surface area, improved porosity, and enhanced catalytic efficiency, have been widely applied in gas adsorption and storage,<sup>7–9</sup> catalysis,<sup>10–13</sup> batteries,<sup>14–17</sup> drug release,<sup>18–21</sup> and supercapacitors.<sup>22–25</sup> However, the electrochemical applicability of a single MOF is limited by shortcomings such as poor water stability, low conductivity, and low mechanical strength. To eliminate these drawbacks, composites with new functions have been developed by combining MOFs with carbon materials,<sup>26–28</sup> metallic nanoparticles (MNPs),<sup>29–31</sup> and metallic oxides.<sup>32</sup>

Table 1 shows the structural formula of MOF in this paper.

# Progress and opportunities for metal–organic framework composites in electrochemical sensors

Wanqing Zhang, <sup>\*a</sup> Xijiao Li,<sup>a</sup> Xiaoman Ding,<sup>a</sup> Kang Hua,<sup>a</sup> Aili Sun,<sup>\*b</sup> Xinxin Hu,<sup>a</sup> Ziwei Nie,<sup>a</sup> Yongsheng Zhang,<sup>c</sup> Jichao Wang, <sup>a</sup> Renlong Li <sup>a</sup> and Shanqin Liu <sup>\*a</sup>

Metal–organic framework composites have the advantages of large surface area, high porosity, strong catalytic efficiency and good stability, which provide a great possibility of finding excellent electrode materials for electrochemical sensors. However, MOF composites still face various challenges and difficulties, which limit their development and application. This paper reviews the application of MOF composites in electrochemical sensors, including MOF/carbon composites, MOF/metal nanoparticle composites, MOF/metal oxide composites and MOF/enzyme composites. In addition, the application challenges of MOF composites in electrochemical sensors are summarized. Finally, the application prospect for MOF composites is considered to promote the synthesis of more MOF composites with excellent properties.

Compared with single MOF and conventional porous materials, modified MOF composites exhibit specific framework structures and diversified functional groups.<sup>33</sup> Electrochemical sensors comprising electrodes modified by MOF composites can effectively recognize metallic ions,<sup>34–37</sup> organic compounds,<sup>38–40</sup> biological molecules,<sup>41–44</sup> and drug molecules,<sup>45–47</sup> thereby improving the detection sensitivity for the target. Bodkhe *et al.*<sup>48</sup> prepared the Au/SWNTs@MOF-199 composite by using MOF-199, Au nanoparticles (AuNPs), and single-walled carbon nanotubes (SWNTs) and developed an electrochemical sensor based on the composite for  $Pb^{2+}$  detection. Under optimized conditions, the detection range and limit

Table 1 An overview of MOF molecular formula in the paper

Materials	Molecular formula	References
Ce-MOF	$Ce_4(bpydc)_6(CH_3O)_4(H_2O)_2$	26
Mn-MOF	$C_{24}H_{40}O_{13}Zn_4$	55
Ni-MOF	$C_8H_6Ni_2O_8$	61
Cr-MOF	$C_{24}H_{17}Cr_3O_{16}$	76
Fe-MOF	$C_{96}H_{64}Cl_2Fe_2N_8O_{32}Zr_6$	29
Cu-BTC MOF	$C_{18}H_{12}Cu_3O_{15}$	141
POMOF	$\{[Mo_5P_2O_{23}][Cu(phen)(H_2O)]_3\cdot 5H_2O\}$	147
ZIF-67	$C_8H_{12}N_4\cdot Co$	107 and 108
ZIF-8	$C_8H_{12}N_4\cdot Zn$	69
UIO-66-NO <sub>2</sub>	$C_{48}H_{22}N_6O_{44}Zr_6$	80
UIO-66-NH <sub>2</sub>	$C_{48}H_{30}N_6O_{32}Zr_6$	119
MIL-101(Fe)	$C_{24}H_{12}ClFe_3O_{13}$	120
MIL-101(Cr)	$C_{24}H_{16}Cr_3FO_{15}$	89
Cu-TCPP	$C_{48}H_{24}N_4O_8Cu\cdot 4\cdot H^+$	57
HKUST-1	$C_{18}H_{12}Cu_3O_{15}$	59
MOF-5	$C_{24}H_{12}O_{13}Zn_4$	86
Zr-MOF	$C_{48}H_{28}O_{32}Zr_6$	97

<sup>a</sup>School of Chemistry and Chemical Engineering, Henan Institute of Science and Technology, Xinxiang, 453003, China. E-mail: zhangwqzzu@163.com; Fax: +86-0373-3040933

<sup>b</sup>School of 3D Printing, Xinxiang University, Xinxiang, 453003, China

<sup>c</sup>China Henan Institute of Advanced Technology, Zhengzhou University, Zhengzhou 450001, China



of detection (LOD) of the sensor for  $\text{Pb}^{2+}$  are  $0.1 \text{ mM}$ – $1 \text{ pM}$  and  $25 \text{ pM L}^{-1}$ , respectively. Owing to its high sensitivity and selectivity, the sensor can be used for wastewater detection. Huang *et al.*<sup>26</sup> proposed an electrochemical sensor based on the Ce-MOF/carbon nanotube (CNT) nano-composite for simultaneous detection of hydroquinone (HQ) and catechol (CC). Owing to the high specific surface area of MOF and good conductivity of CNT, the developed sensor shows excellent electrochemical performance for HQ and CC detection, with linear ranges of  $10$ – $100$  and  $5$ – $50 \mu\text{M}$ , respectively; therefore, the sensor can also be used for detecting environmental pollutants.

Tang *et al.*<sup>49</sup> modified a glassy carbon electrode (GCE) using the prepared GO-ZIF-67 composite *via* electrodeposition, and developed the GO-ZIF-67/GCE electrochemical sensor for detecting dopamine (DA) and uric acid (UA); thus, the sensor showed excellent electrochemical performance for DA and UA detection, owing to the synergistic effect of the high conductivity of GO and high profitability of ZIF-67. Li *et al.*<sup>50</sup> synthesized ZIF-65 and prepared an electrochemical sensor by combining ZIF-65 with carboxylated CNTs for detecting ascorbic acid (AA). The introduction of carboxylated carbon nanotubes increased the conductivity of the electrochemical sensor and accelerated the transfer of electrons between the sensor and the target molecules. In addition, the exposed nitro group in MOF can be utilized as the redox active sites, so that the composite material has good water stability and large internal volume, which is helpful to improving the sensitivity and reproducibility

of the constructed sensor. Under optimal conditions, the detection range and LOD of this sensor for AA are  $200$ – $2267 \text{ mM}$  and  $1.03 \text{ mM}$ . In summary, MOF composites show good molecular detection performance for wastewater, environmental pollutants, and drugs and can serve as a potential material for the development of electrochemical sensors.

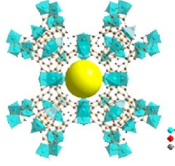
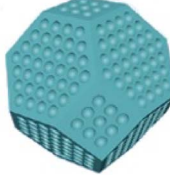
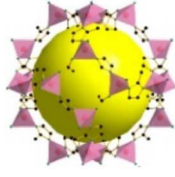
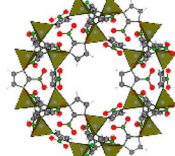
The structure, metal ions and ligands of MOF involved in the Introduction section are shown in Table 2.

In this study, multiple MOF composites for electrochemical sensing, including MOF/carbon, MOF/MNPs, and MOF/metallic oxides (Fig. 1) are reviewed. Furthermore, the excellent applicability of MOF composites for the development of electrochemical sensors is discussed, and future applications of these composites have been presented. This paper also provides references to different applications of MOF composites.

## 2. MOF/carbon composite

Carbon materials (*e.g.*, carbon fiber, graphene, carbon nanotubes, XC-72), which are characterized by good conductivity, large specific surface area, and diverse functional groups, have been applied in supercapacitors, electrocatalysis, and batteries.<sup>51–54</sup> Composites comprising MOF and carbon materials exhibit high porosity, large specific surface area, and high catalytic efficiency (attributed to MOF) as well as good conductivity (attributed to carbon materials); thus, these are widely applied in electrochemical sensing (Table 3).

Table 2 An overview of MOF structures and their basic constituents

MOF identify	MOF structure	Metal ion	Ligand	Reference
MOF-199		$\text{Cu}^{2+}$	$\text{H}_3\text{BTC}$	48
Ce-MOF		$\text{Ce}^{2+}$	$\text{H}_3\text{BTC}$	26
ZIF-67		$\text{Co}^{2+}$	2-Methylimidazole	49
ZIF-65		$\text{Zn}^{2+}$	2-Methylimidazole	50



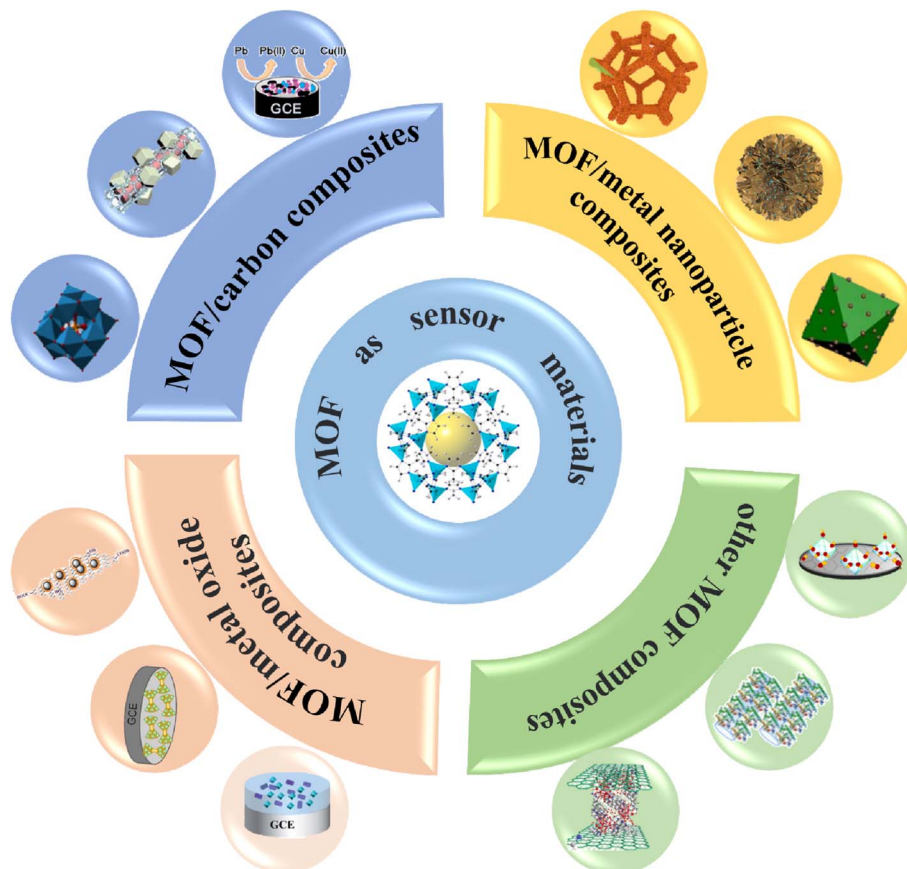


Fig. 1 Application of MOF composites in electrochemical sensors.

## 2.1 MOF/carbon nanotubes composite

CNTs are seamless cylindrical tubes made of single or multi-layer graphite sheets, which are hybridized with  $sp^2$  carbons and coiled around the central axis at a specific helix angle. Examples include SWCNTs and multi-walled carbon nanotubes (MWCNTs), which are characterized by large specific surface area, high conductivity, and good chemical stability. Consequently, composites comprising with MOF and CNTs have been

used for the development of electrochemical sensors with high sensitivity and high selectivity.<sup>65–68</sup>

Rani *et al.*<sup>39</sup> prepared the Sn-MOF@CNT composite (Fig. 2(a)) using a solvothermal method. The constructed Sn-MOF has a porous structure and large specific surface area, while CNTs can provide rapid electron transfer channels. Electrochemical sensors comprising Au electrodes modified by the Sn-MOF@CNT composite exhibited excellent performance for

Table 3 Application of MOF/carbon composites in electrochemical sensors

MOF composites	Target analysis	Linear range	Limit of detection (LOD)	References
Mn-MOF/SWCNTs	$Pb^{2+}$	0.10–14.0 $\mu$ M	38 nM	55
MIL-101/MWCNTs	Picloram	0.1–12.5 $\mu$ M 12.5–40 $\mu$ M	0.06 $\mu$ M	56
Cu-TCPP/CNT	$H_2O_2$	0.01–377.75 $\mu$ M	5 nM	57
ZIF-8/GN	Dopamine	0.003–1.0 mM	1.0 $\mu$ M	58
HKUST-1/RGO	Nitrite	3–40000 $\mu$ M	33 nM	59
HKUST-1/ERGO	Adenine	0.02–100 $\mu$ M	0.012 $\mu$ M	60
	Guanine	0.005–200 $\mu$ M	0.002 $\mu$ M	
Ni-MOF/SWCNT	Glucose	20 $\mu$ M–4.4 mM	4.6 $\mu$ M	61
HKUST-1/MWCNTs	Metformin	0.5–25 $\mu$ M	0.12 $\mu$ M	62
Zn/Ni-ZIF-8/XC-72/Nafion	$Pb^{2+}$	0.794–39.6 ppm	0.0150 ppm	63
	$Cu^{2+}$	0.397–19.9 ppm	0.0096 ppm	
MIL-101(Cr)/XC-72	Chloramphenicol	0.01–20 $\mu$ M	1.5 nM	64



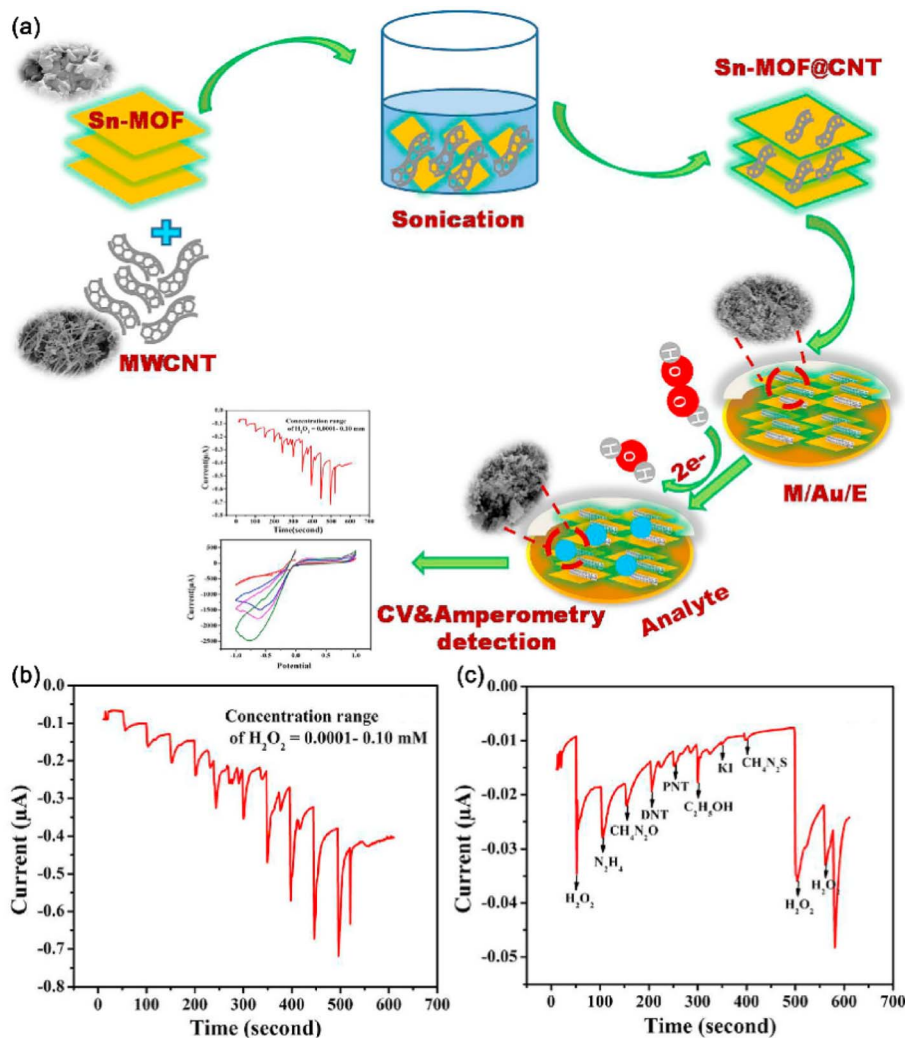


Fig. 2 (a) Detection of H<sub>2</sub>O<sub>2</sub> by the electrochemical sensor based on the Sn-MOF@CNT composite; (b) *i*-*t* curves obtained by adding H<sub>2</sub>O<sub>2</sub> solution with different concentrations to the Sn-MOF@CNT/Au sensor every 50 s; (c) specificity of the Sn-MOF@CNT/Au sensor toward H<sub>2</sub>O<sub>2</sub>. Reprinted with permission from ref. 39. Copyright 2020 Environment Research.

electrochemical detection of H<sub>2</sub>O<sub>2</sub>. Different H<sub>2</sub>O<sub>2</sub> concentrations are added into a 0.1 M phosphate buffered solution (PBS; pH = 7.4), and the reported sensor shows an excellent current response to the target molecules; in the presence of interfering substances (hydrazine, urea, DNT, pNT, ethanol, KI, thiourea), the Sn-MOF@CNT/Au sensor shows no significant peak currents, indicating its good specificity.

Qin *et al.*<sup>69</sup> developed the ZIF-8/MWCNTs/GCE electrochemical sensor for detecting rutin. Specifically, the ZIF-8/MWCNTs composite was prepared *via in situ* synthesis, wherein ZIF-8 nanoparticles were deposited on MWCNTs (Fig. 3(a)). Owing to the synergistic effect of ZIF-8 and MWCNTs, the composite provides abundant active centers for the target molecules, and improves the electron transfer capability of the electrochemical sensors. Consequently, the differential pulse voltammetry (DPV) peak current of ZIF-8/MWCNTs/GCE is significantly higher than those of MWCNTs/GCE and bare GCE (Fig. 3(b)). Fig. 3(c) shows that the peak current of rutin linearly increases with a rise in the scanning rate in the range of 20–

200 mV s<sup>-1</sup>, indicating that the rutin reaction on the electrode surface is a typical adsorption-controlled process. Additionally, this electrochemical sensor exhibits excellent performance for rutin detection in real-world samples.

## 2.2 MOF/graphene composite

As a natural 2D carbon material, graphene has a honeycombed structure and exhibits high conductivity, excellent electrocatalytic activity, large specific surface area, and good biocompatibility. Consequently, graphene has been widely applied in electrochemical sensors and biosensors.<sup>70–73</sup> The presence of graphene can accelerate electron transfer in MOF composites, thereby enhancing the conductivity and electrochemical activity of MOF/graphene composites.<sup>74</sup>

Li *et al.*<sup>75</sup> developed an electrochemical sensor based on the Cu-based metal–organic framework-graphene composite (Cu-MOF-GN) for simultaneous detection of HQ and CT. Owing to the large specific surface area and good adsorbability of Cu-

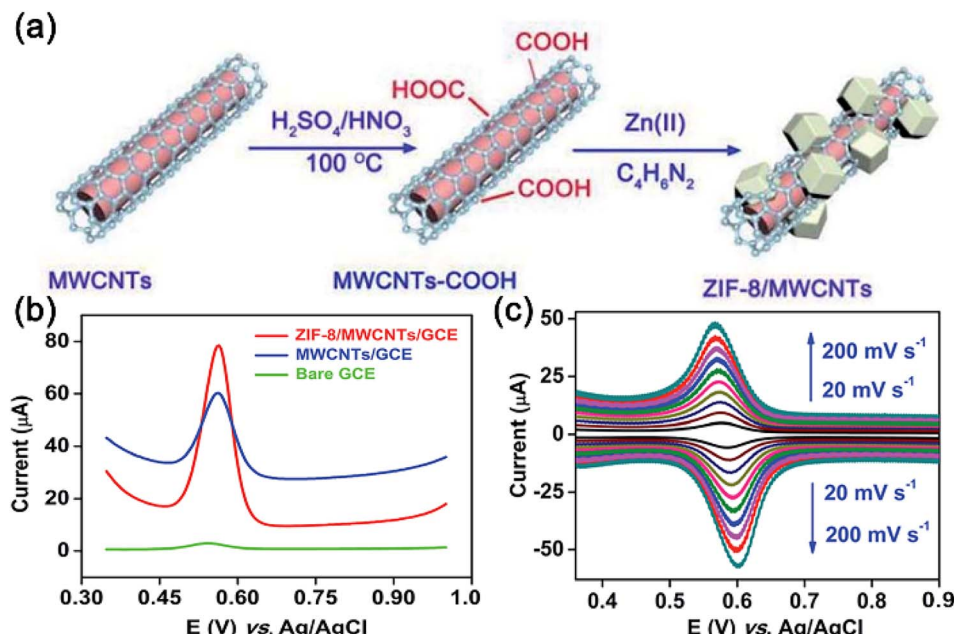


Fig. 3 (a) Preparation of the ZIF-8/MWCNTs composite; (b) CV curves for 5 mM rutin generated by the bare GCE, MWCNTs/GCE, and ZIF-8/MWCNTs/GCE sensors; (c) electrochemical response of the ZIF-8/MWCNTs/GCE sensor to rutin at different scanning rates. Reprinted with permission from ref. 69. Copyright 2021 Analytical Methods.

MOF, as well as the excellent conductivity and stability of GN, the Cu-MOF-GN/GCE sensor exhibits excellent electrocatalytic performance for detecting HQ and CT. The recovery rate achieved by this sensor for the detection of HQ and CT in tap water is 99.0–102.9%, and the RSD is below 5% for five consecutive replicates; this indicates that this composite can be used for detecting HQ and CT in real-world samples.

Cui *et al.*<sup>76</sup> introduced dendrimer polyamidoamine (PAMAM) and ERGO into the synthesis process of Cr-MOF material, which

made the prepared composites have good crystallinity, small size and large specific surface area. The hydrogen link and  $\pi-\pi$  bond synergistically improved the electrical conductivity of PAMAM/Cr-MOF/ERGO composite, increasing the electrochemical active area and sensing sensitivity of the constructed sensors. Under optimized conditions, the linear ranges and LOD of sensor for 1-OHPyr are 0.1–6.0  $\mu M$  and 0.075  $\mu M$ , respectively. Additionally, this sensor exhibits good selectivity, reproducibility, and stability. This study provides experimental

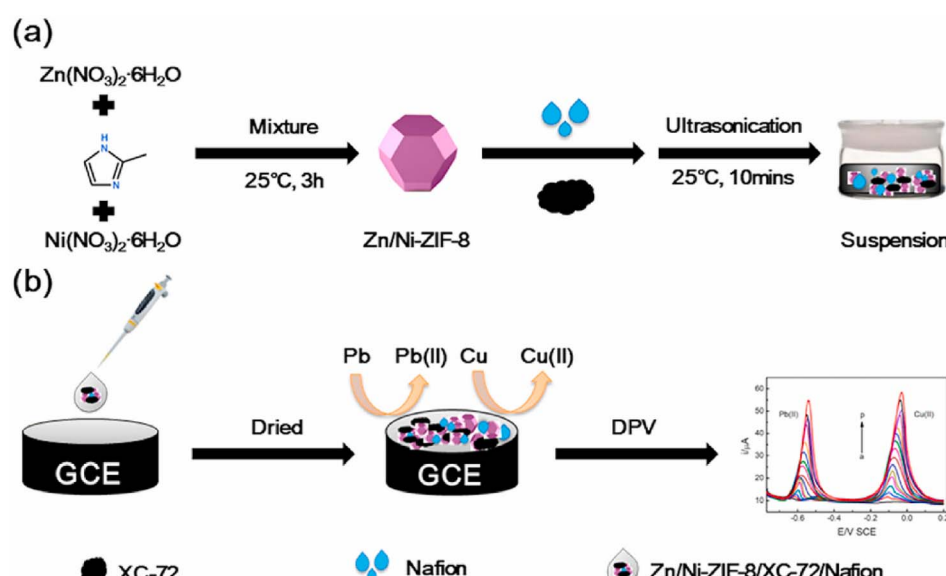


Fig. 4 (a) Preparation of the Zn/Ni-ZIF-8/XC-72/Nafion suspension; (b) detection of Pb(II) and Cu(II) using the Zn/Ni-ZIF-8/XC-72/Nafion/GCE sensor. Reprinted with permission from ref. 64. Copyright 2021 Environmental Research.



references for the development and application of electrochemical sensing platforms.

Zeng *et al.*<sup>77</sup> developed the Cu-MOF/Fe<sub>3</sub>O<sub>4</sub>-GO/GCE electrochemical sensor by modifying GCE with the as-prepared Cu-MOF/magnetic Fe<sub>3</sub>O<sub>4</sub>-graphene oxide (Fe<sub>3</sub>O<sub>4</sub>-GO) composite for rapid detection of zearanene (ZEA) in breakfast cereals, corn flour, and rice flour. As indicated by the density functional theory (DFT), Cu-MOF on the Fe<sub>3</sub>O<sub>4</sub>-GO surface promotes electron transfer between energy bands, thereby facilitating rapid oxidation of ZEA on the sensor surface. Additionally, this sensor shows excellent stability, high selectivity, a wide linear range (159.2–2865.2 ng mL<sup>-1</sup>), and a low LOD (23.14 ng mL<sup>-1</sup>).

### 2.3 MOF/XC-72 composite

XC-72, which is known for its large specific surface area, excellent thermal stability, outstanding conductivity, and good biocompatibility, has been employed for loading MOF materials.<sup>78,79</sup> Currently, the MOF/XC-72 composites have been widely used for electrochemical detection of target molecules.

Li *et al.*<sup>64</sup> developed a novel electrochemical sensor by using the Zn/Ni-ZIF-8/XC-72/Nafion composite as an electrode surface modifier for simultaneous detection of Pb(II) and Cu(II) (Fig. 4). Owing to the large specific surface area of Zn/Ni-ZIF-8 and high conductivity of XC-72, the Zn/Ni-ZIF-8/XC-72/Nafion/GCE sensor exhibits excellent electrochemical response for Pb(II) detection (0.794–39.6 ppm) and Cu(II) (0.397–19.9 ppm), with LODs of 0.0150 and 0.0096 ppm, respectively. Additionally, this sensor shows a good recovery rate for the detection of heavy metal ions in lake water and honey, thereby demonstrating its excellent potential for simultaneously detecting multiple heavy metal ions in real-world samples.

Zhang *et al.*<sup>80</sup> developed the UIO-66-NO<sub>2</sub>@XC-72/GCE electrochemical sensor by modifying GCE with the UIO-66-NO<sub>2</sub>@XC-72 composite *via* hydrothermal synthesis for simultaneous detection of AA, DA and UA (Fig. 5). Individual and simultaneous detection of AA, DA and UA are achieved by using the DPV method. Due to the large surface area of UIO-66-NO<sub>2</sub>,

good conductivity of XC-72 and hydrogen bonding between UIO-66-NO<sub>2</sub> and the target analyte, the composite is very suitable to be used as sensor modifier. The oxidation peak current of this sensor exhibits excellent linearity with the concentration of target molecules; the detection ranges of AA, DA and UA are 0.2–3.5, 0.03–2.0 and 0.75–22 mM, respectively, and the LODs of AA, DA and UA are 0.12, 0.05, and 0.03 mM (S/N = 3), respectively. Overall, this sensor delivers promising results for detection of AA, DA and UA in real-world samples.

## 3. MOF/MNPs composite

Owing to their unique electronic structure, high chemical activity, and special size and shape, MNPs have attracted considerable attention.<sup>81,82</sup> Combined with MOF, MNPs can promote the conductivity of MOF and significantly improve the catalytic performance of the MOF/MNPs composite. By modifying the electrode, the constructed electrochemical sensor can sensitively and efficiently detect the target molecules. However, the applicability of MNPs has been severely limited by agglomeration and poor stability. These drawbacks can be eliminated by encapsulating MNPs into nano-cavities or open channels of MOF.<sup>83</sup> Additionally, MOF/MNPs composites have been widely applied in electrochemical sensor owing to their good conductivity as well as optical and catalytic performances<sup>84,85</sup> (Table 4).

### 3.1 MOF/Au nanoparticles (AuNPs) composite

Owing to their good conductivity, AuNPs can significantly reduce the distance between electron donors and acceptors, and accelerate the transfer of electrons to the electrode surface, thereby enhancing selectivity and sensitivity of the corresponding sensors.<sup>94–96</sup> The presence of MOF can control the size of AuNPs and prevent agglomeration of the composite. Hence, MOF/AuNPs composites can be used in a wide range of applications for improving the performance of modified electrodes.

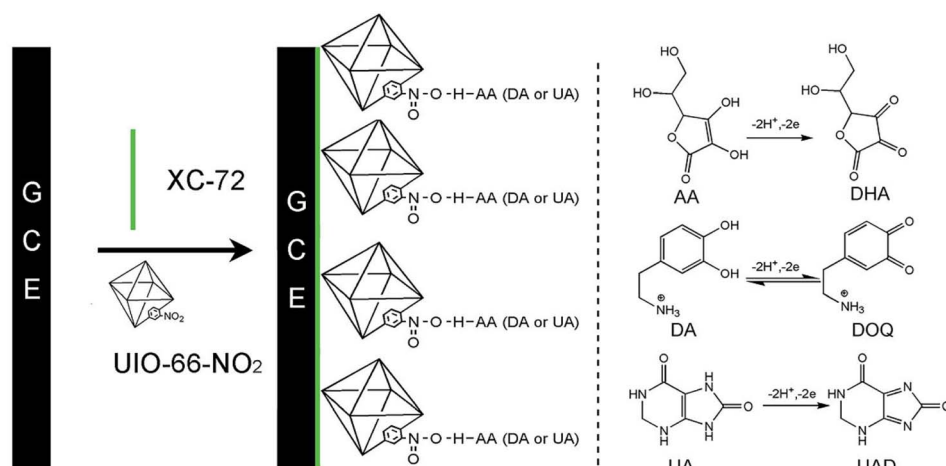


Fig. 5 Preparation of the UIO-66-NO<sub>2</sub>@XC-72/GCE sensor and the corresponding mechanisms governing redox reactions of AA, DA and UA. Reprinted with permission from ref. 80. Copyright 2017 RSC Advances.



Table 4 Application of MOF/MNPs in electrochemical sensors

MOF composites	Target analysis	Linear range	Limit of detection (LOD)	References
Au-MOF-5	Nitrobenzene nitrite	20 $\mu$ M–6.0 mM 5.0 $\mu$ M–65 mM	15.3 $\mu$ M 1.0 $\mu$ M	86
Ag@MOF-5(Zn)	2-Nitrophenol	0.1–10 $\mu$ M 50–200 $\mu$ M	0.09 $\mu$ M	87
Ag@ZIF-67	Glucose	2–1000 $\mu$ M	0.66 $\mu$ M	88
Pt@MIL-101(Cr)	Xanthine	0.5–162 $\mu$ M	0.42 $\mu$ M	89
AuPd/UiO-66-NH <sub>2</sub>	Nitrite	0.05–5666 $\mu$ M	0.01 $\mu$ M	90
Au/Cu-MOF	Nitrite	0.1 $\mu$ M–10 mM	82 nM	91
Pt@UIO-66-2	Hydrazine	0.05–4017.6 $\mu$ M	0.024 $\mu$ M	92
Cu-in-ZIF-8	Glucose	0–0.7 mM	2.76 $\mu$ M	93

Sun *et al.*<sup>97</sup> developed a voltammetric detection method for sensitive analysis of sunset yellow (SY) and Sudan I based on AuNPs/Zr-MOF-graphene composite modified GCE. The prepared composite not only has the benefits of a single material, but also can prevent the disordered aggregation of AuNPs on MOF material, greatly enhancing the analytical performance of the sensor toward SY and Sudan I. The excellent electrochemical performance can be ascribed to the high catalytic activity of AuNPs/Zr-MOF and the quick electron transfer rate of graphene. Under the optimal conditions, the constructed sensor has wide linear range (0.1–1000  $\mu$ M and 0.1–800  $\mu$ M) and low detection limits (0.1  $\mu$ M and 0.1  $\mu$ M). In addition, the AuNPs/Zr-MOF-Graphene/GCE sensor has also been successfully applied to the real detection of SY in beverages and Sultan I in chili powder, and obtained satisfactory recoveries (92.89–109.87%). The above results indicate that the sensor has great potential application in the detection of azo dyes (Fig. 6).

Hatamluyi *et al.*<sup>98</sup> developed a highly sensitive molecular imprinting electrochemical sensor for detecting patulin (Fig. 7). Specifically, GCE was modified with N-doped graphene quantum dots (N-GQDs) and Au@Cu-MOF, and the MIP/

Au@Cu-MOF/N-GQDs/GCE electrochemical sensor was developed using electropolymerization. The presence of N-GQDs significantly enhanced sensing conductivity, and the unique structure of Au@Cu-MOF significantly increased the number of binding sites on the polymer. This sensor exhibits a wide linear range (0.001–70.0 ng mL<sup>−1</sup>) and low LOD (0.0007 ng mL<sup>−1</sup>) for patulin, as well as good selectivity, stability and reproducibility. This sensor shows promising recovery rates (97.6–99.4%) for patulin detection in apple juice, suggesting that it can be used for rapid detection of patulin in real-world samples.

Dang *et al.*<sup>99</sup> prepared the AuNPs-NH<sub>2</sub>/Cu-MOF composite by grafting ammoniated AuNPs (AuNPs-NH<sub>2</sub>) to Cu-MOF, and developed the AuNPs-NH<sub>2</sub>/Cu-MOF/GCE sensor for detecting H<sub>2</sub>O<sub>2</sub>. The recognition of H<sub>2</sub>O<sub>2</sub> by the fabricated sensor was carried out as following: through the reversible reaction between Cu<sub>2</sub>O and CuO in MOF material, the electron was captured by H<sub>2</sub>O<sub>2</sub>, and then the corresponding electrochemical reduction reaction occurred, resulting in the formation of OH and H<sub>2</sub>O. This sensor shows a wide linear range (5–850  $\mu$ M), low LOD (1.2  $\mu$ M), and high sensitivity (1.71  $\mu$ A cm<sup>−2</sup>  $\mu$ M<sup>−1</sup>). Consequently, the AuNPs-NH<sub>2</sub>/Cu-MOF/GCE electrochemical

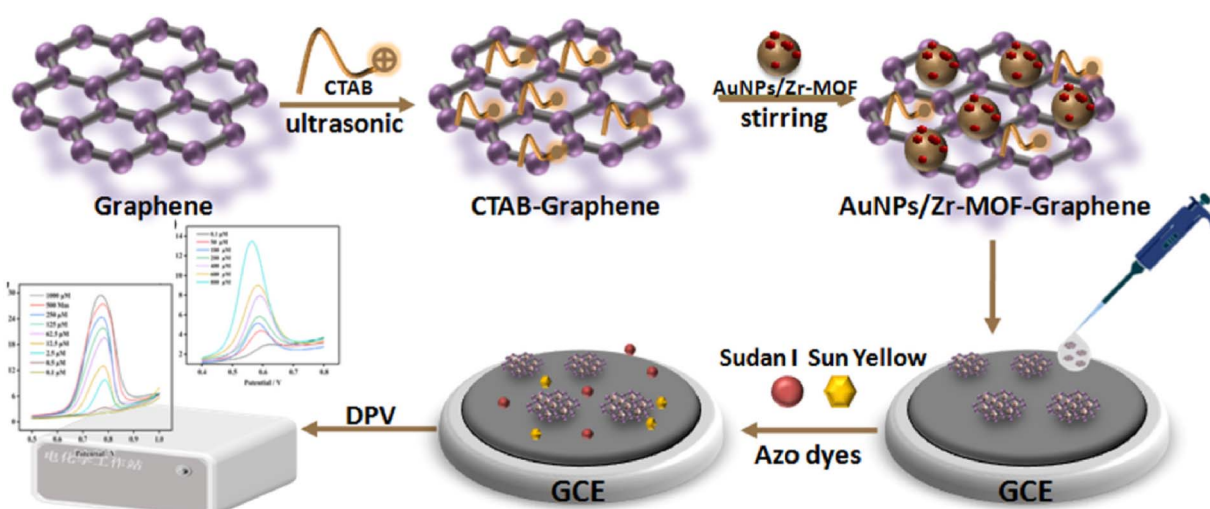


Fig. 6 Detection of SY and Sudan I using the AuNPs/Zr-MOF-Graphene/GCE sensor. Reprinted with permission from ref. 97. Copyright 2022 Food Control.



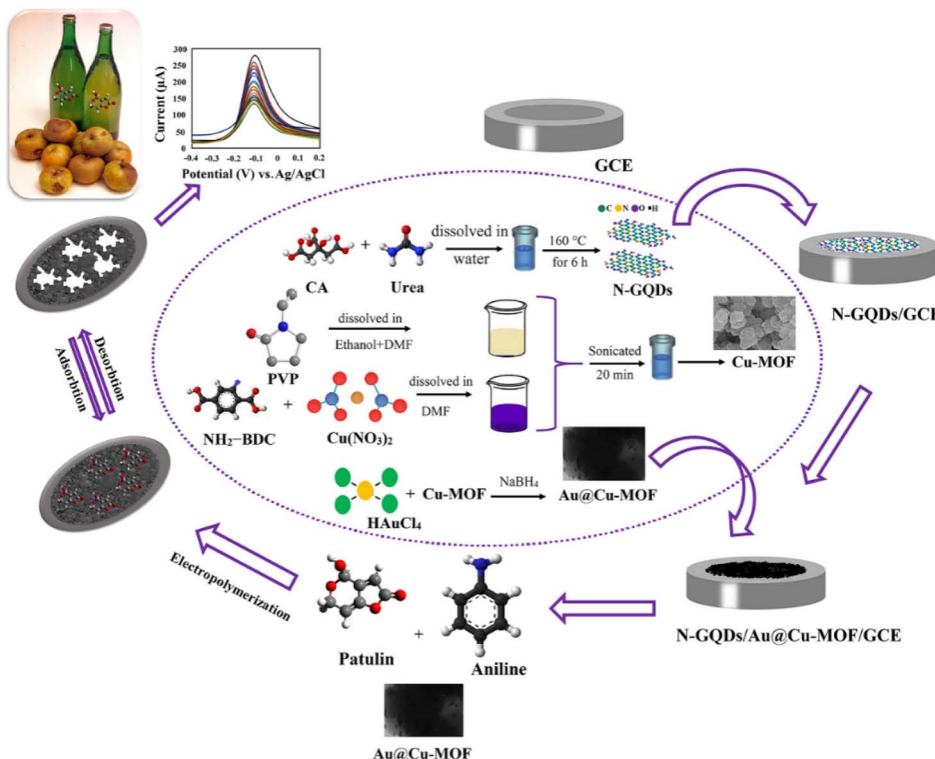


Fig. 7 Development of the MIP/Au@Cu-MOF/N-DGQs/GCE sensor and application for patulin detection. Reprinted with permission from ref. 98. Copyright 2020 Sensors and Actuators B: Chemical.

sensor is highly promising for detecting  $\text{H}_2\text{O}_2$  released by HeLa cells. Sun *et al.*<sup>100</sup> established the ZIF-8/AuNPs/PVP-rGO/GCE electrochemical sensor by modifying a GCE with polyvinylpyrrolidone (PVP)-dispersed reduced graphene oxide (PVP-rGO), AuNPs, and ZIF-8 for highly sensitive detection of salbutamol (SAL). Herein, the porous structure of ZIF-8 facilitates SAL adsorption on the modified electrode. Meanwhile, the synergistic effect of PVP-rGO and AuNPs, both of which have excellent conductivity, significantly enhance the electrochemical activity of the sensor. Compared with conventional sensors, this sensor shows superior electrochemical performance, with the linear detection range and LOD for SAL being 0.001–5 nM and 0.001 nM, respectively. Additionally, this electrochemical sensor exhibits excellent recovery rates (94.0–107.0%) for SAL detection in pork.

### 3.2 MOF/Ag nanoparticles (AgNPs) composite

AgNPs are characterized by low costs, low toxicity, and good catalytic performance. The abundant active sites on the surface of AgNPs can promote electron transfer.<sup>101,102</sup> Electrode modification with the MOF/AgNPs composite prevents agglomeration of AgNPs in the solution, amplifies the current signals, and enhances the electron transfer rate, thereby achieving highly sensitive detections.<sup>103–105</sup>

Tang *et al.*<sup>106</sup> prepared an Ag-doped CoNi MOF (Ag–CoNi-MOF) composite and developed the Ag–CoNi-MOF/GCE electrochemical sensor for detecting luteolin by modifying GCE with this composite (Fig. 8). The Ag–CoNi-MOF composite

exhibits high specific surface area and conductivity, thereby providing abundant active sites for luteolin. Under optimized experimental conditions, electrochemical detection of luteolin was conducted using the DPV method with high sensitivity. The results demonstrate that the DPV method shows a good linearity in the range of 0.002–1.0  $\mu\text{M}$ , while exhibiting an LOD of 0.4 nM ( $\text{S}/\text{N} = 3$ ). Additionally, this sensor shows a good performance for luteolin detection in human urine samples, with high selectivity and sensitivity.

Dong *et al.*<sup>107</sup> prepared the Ag@ZIF-67 composite by encapsulating AgNPs into ZIF-67 at room temperature, and then developed the Ag@ZIF-67/GCE sensor for detecting  $\text{H}_2\text{O}_2$ . Owing to the synergistic effect of Ag and ZIF-67, the Ag@ZIF-67/GCE sensor exhibits electrocatalytic activity toward  $\text{H}_2\text{O}_2$ . This sensor has three linear ranges for detecting  $\text{H}_2\text{O}_2$  (5.0–275  $\mu\text{M}$ , 775–2775  $\mu\text{M}$  and 4775–16775  $\mu\text{M}$ ), while exhibiting an LOD of 1.5  $\mu\text{M}$ . Additionally, this sensor shows good stability, reproducibility and specificity. It also exhibits high recovery rates for detection of real-world samples of  $\text{H}_2\text{O}_2$  disinfectants, suggesting that Ag@ZIF-67 can be used for development of electrochemical sensors.

Fan *et al.*<sup>108</sup> constructed an electrochemical sensor for  $\text{Cl}^-$  sensitive detection using ZIF-67/AgNPs/polydopamine (PDA) composite with yolk-shell structure and diameter of 400–600 nm as the modification material of GCE (Fig. 9). As a protective layer, the PDA coating greatly decreases the release of AgNPs from the ZIF-67 substrate and provides a more stable electrochemical response for the determination of  $\text{Cl}^-$ . This



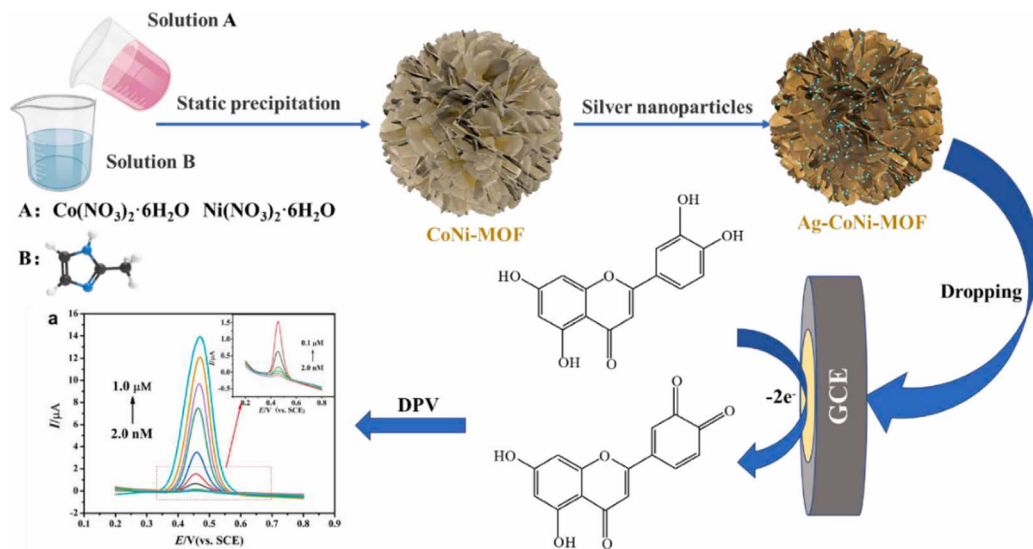


Fig. 8 Development of the Ag–CoNi-MOF/GCE sensor and application in electrochemical detection of luteolin. Reprinted with permission from ref. 106. Copyright 2022 Microchemical Journal.

electrochemical sensor exhibits promising recovery rates (93.37–109.85%) for  $\text{Cl}^-$  detection in artificial sweat samples. Meanwhile, the ZIF-67/AgNPs/PDA/GCE sensor exhibits high sensitivity, selectivity and stability for  $\text{Cl}^-$  detection.

Saedi *et al.*<sup>109</sup> prepared the AgNPs/CuMOF/PPy-rGO composite using the hydrothermal method and developed an electrochemical sensor for detecting metronidazole (MTZ) by employing a carbon-pasted electrode (CPE) modified by the AgNPs/CuMOF/PPy-rGO composite as the working electrode (Fig. 10). The AgNPs/CuMOF/PPy-rGO composite amplifies the electrochemical signals of the developed sensor and decreases LOD. For the B-R buffer containing MTZ, the linear range and LOD of this sensor are 0.08–160  $\mu\text{M}$  and 24 nM, respectively. Additionally, this sensor shows excellent sensitivity and

selectivity for the detection of MTZ in tablets and human urine samples, thereby demonstrating the excellent potential of this composite in antibiotic monitoring.

### 3.3 MOF/Pt nanoparticles (PtNPs) composite

PtNPs are characterized by higher catalytic activities compared to those of other noble metal NPs. Hence, encapsulation of PtNPs in MOF has been prevalent in electrochemical sensing as it can effectively control the size of PtNPs and improve catalytic activity and selectivity.<sup>110–112</sup>

Zhang *et al.*<sup>89</sup> developed a non-enzyme electrochemical platform for detection of xanthine (XA). Herein, MIL-101 (Cr) with a porous cage structure and large specific surface area was employed as the framework for loading PtNPs (Fig. 11). Owing

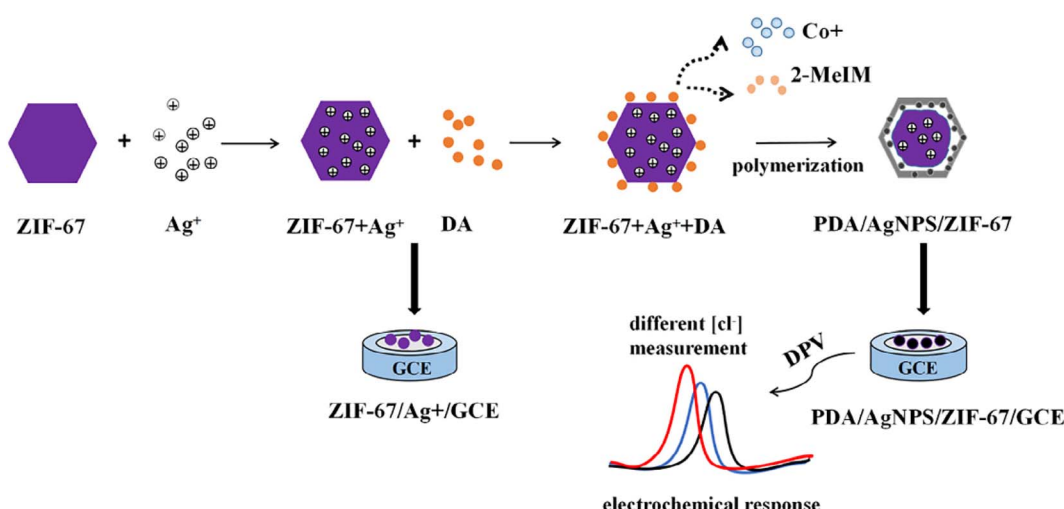


Fig. 9 Preparation of the ZIF-67/AgNPs/PDA/GCE sensor and electrochemical detection of  $\text{Cl}^-$ . Reprinted with permission from ref. 108. Copyright 2022 Journal of Electroanalytical Chemistry.

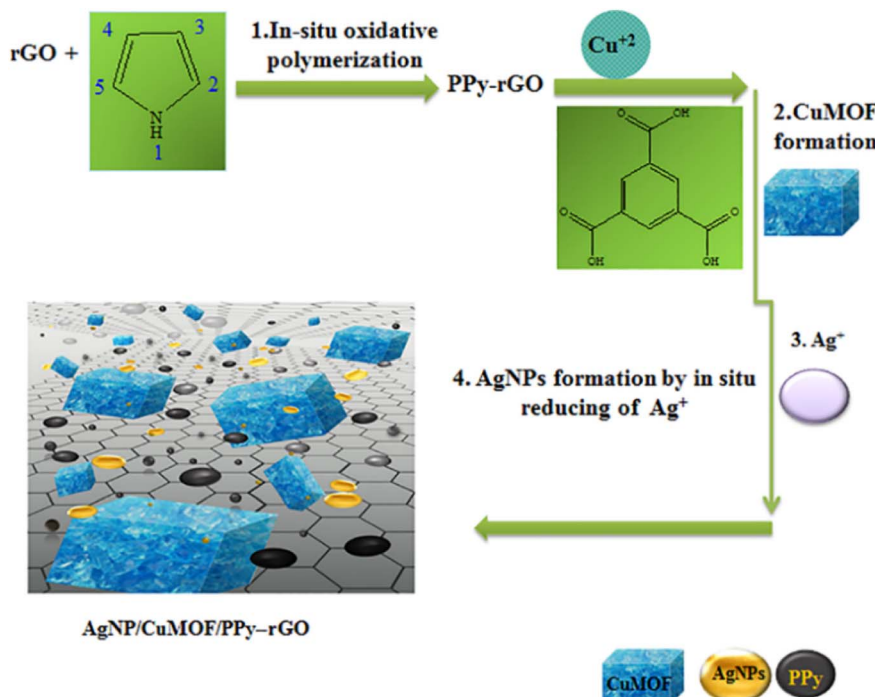


Fig. 10 Preparation of AgNPs/CuMOF/PPy-rGO nano-composites. Reprinted with permission from ref. 109. Copyright 2021 Journal of the Chinese Chemical Society.

to the ordered crystal structure and large specific surface area of MIL-101 (Cr) as well as the high conductivity of PtNPs, this sensor shows excellent sensing performance for XA, with a linear range of 0.5–162  $\mu$ M and LOD of 0.42  $\mu$ M. Additionally, the Pt@MIL-101(Cr)/GCE electrochemical sensor delivers promising recovery rates (100.80–103.00%) for XA detection in human serum samples.

Saeb *et al.*<sup>29</sup> reported the Fe-MOF/PtNPs/GCE sensor for detecting tinidazole (TDZ). The electrochemical performance of

the Fe-MOF/PtNPs/GCE sensor was investigated using the DPV method. The Fe-MOF/PtNPs composite increases the number of electrocatalytic active sites for TDZ and facilitates electron transfer between the electrode and TDZ. Thus, this sensor exhibits a wide linear range (0.02–525  $\mu$ M), low LOD (43 nM), good selectivity and excellent stability. Additionally, it also shows high recovery rates (98.28–108.33%) for TDZ detection in human plasma.

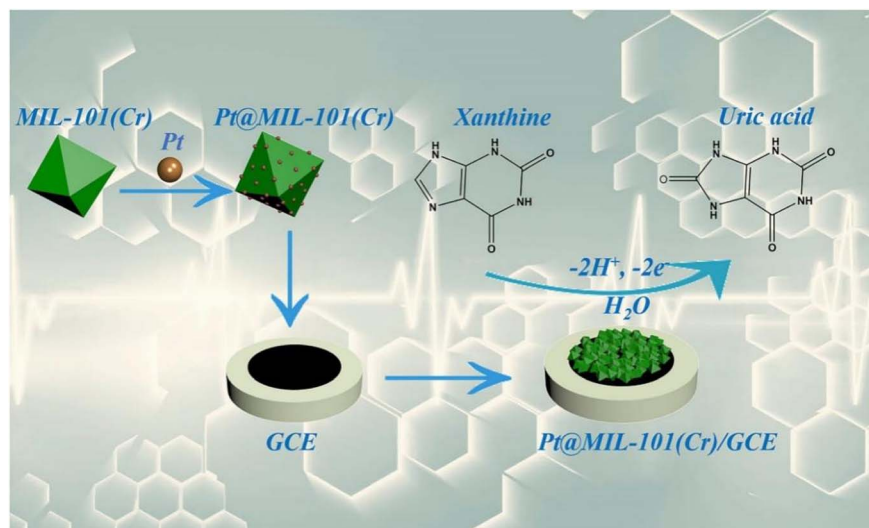


Fig. 11 Mechanism of molecular recognition of XA at the Pt@MIL-101(Cr)/GCE sensor. Reprinted with permission from ref. 89. Copyright 2018 Microchimica Acta.



## 4. MOF/metallic oxides composite

Metallic oxides have attracted considerable attention owing to their good catalytic performance, unique magnetism and excellent photoelectric characteristics.<sup>113–116</sup> Metallic oxides (e.g., CuO, ZnO, Al<sub>2</sub>O<sub>3</sub>, Fe<sub>3</sub>O<sub>4</sub>, and TiO<sub>2</sub>) mostly belong to semiconductor material. When they are combined with MOF, the materials can strengthen their dispersion in MOF/metal oxides composites. In addition, the large surface area and abundant active sites of the prepared composites can provide a microenvironment suitable for the electrochemical reaction of target molecules, which is helpful to the effective identification and rapid detection of target object<sup>117,118</sup> (Table 5).

### 4.1 MOF/Fe<sub>3</sub>O<sub>4</sub> composite

Owing to their large specific surface area, abundant active centers, high catalytic efficiency, and good adsorption capacity, magnetic nano-materials have been thoroughly investigated and widely applied.<sup>125–127</sup> Fe<sub>3</sub>O<sub>4</sub> is one of the most widely used magnetic nano-materials because MOF/Fe<sub>3</sub>O<sub>4</sub> composites exhibit the synergistic effect of MOF and Fe<sub>3</sub>O<sub>4</sub>, and can effectively prevent agglomeration of these composites. Consequently, MOF/Fe<sub>3</sub>O<sub>4</sub> composites show excellent potential for electrochemical sensing.

Chang *et al.*<sup>128</sup> polymerized DA onto the surface of Fe<sub>3</sub>O<sub>4</sub> nanoparticles, and then combined it with CuSO<sub>4</sub> and H<sub>3</sub>BTC to prepare magnetic Fe<sub>3</sub>O<sub>4</sub>@PDA@MOF material, which was applied to construct Fe<sub>3</sub>O<sub>4</sub>@PDA@MOF@MIP electrochemical sensor for detecting oxytetracycline. The introduction of MOF can increase the surface area of Fe<sub>3</sub>O<sub>4</sub> nanoparticles, thus increasing the number of pores and effective binding sites of MIP, so that the sensor has an obvious electrochemical response to tetracycline. Moreover, the fabricated sensor also exhibits wide linear range, good reproducibility and strong anti-interference ability, and can perform highly sensitive detection of tetracycline in milk samples.

Salman *et al.*<sup>129</sup> prepared the MIL-101(Fe)@Fe<sub>3</sub>O<sub>4</sub> composite and developed an electrochemical sensor by modifying GCE with the MIL-101(Fe)@Fe<sub>3</sub>O<sub>4</sub> composite for detecting H<sub>2</sub>O<sub>2</sub>. Compared with bare GCE, the MIL-101(Fe)@Fe<sub>3</sub>O<sub>4</sub>/GCE sensor shows excellent electrochemical activity during electrocatalytic reduction of H<sub>2</sub>O<sub>2</sub> as it provides effective electron transfer channels for target molecules. Under optimized conditions, the oxidation peak current has a good linearity with the H<sub>2</sub>O<sub>2</sub> concentration (5–55 μM), an LOD of 0.15 μM (S/N = 3), and

a sensitivity of 68.8312 μA mM<sup>−1</sup> cm<sup>−2</sup>. Additionally, this sensor shows good reproducibility, long-term stability and high selectivity.

Wang *et al.*<sup>121</sup> prepared the Fe<sub>3</sub>O<sub>4</sub>@ZIF-8/rGO composite and developed the Fe<sub>3</sub>O<sub>4</sub>@ZIF-8/rGO/GCE sensor by modifying GCE with the Fe<sub>3</sub>O<sub>4</sub>@ZIF-8/rGO composite for highly sensitive detection of DA (Fig. 12). Owing to large specific surface area of MOF and high conductivity of graphene, this composite shows high electrocatalytic activity for DA detection. Under optimized conditions, the oxidation peak current of DA during the DPV method has a good linearity (2 nM–10 μM) and an LOD of 0.667 nM. Thus, this method is optimal for electrochemical detection of DA.

### 4.2 MOF/ZnO composite

ZnO is a key wide-bandgap semiconductor material that has been widely utilized in photocatalytic, drug delivery and sensor. However, vacancies and defects of ZnO can barely be controlled during preparation process. Consequently, stability and catalytic efficiency of ZnO often fall short of the demand.<sup>129–131</sup> Recently, MOF/ZnO composite enhanced the catalytic performance of ZnO and diversified the functions of MOF, resulting in widespread use of this composite for sensing.

Li *et al.*<sup>132</sup> prepared the UIO-66-NH<sub>2</sub>/ZnO nano-composite with stabilized performances *via* ultrasonic mixing of UIO-66-NH<sub>2</sub> and ZnO, and then developed an electrochemical sensor for detecting Cu<sup>2+</sup> (Fig. 13). This composite has abundant –OH and –NH<sub>2</sub>, thereby providing plentiful active sites for Cu<sup>2+</sup>. Under optimized conditions, this sensor has a good linearity (0.2–0.9 μM), an LOD of 0.01435 mM and a sensitivity of 6.46 μA μM<sup>−1</sup>. Additionally, this sensor shows excellent performance for rapid detection of Cu<sup>2+</sup> in real-life water samples.

Guo *et al.*<sup>122</sup> developed the ZnO@ZIF-8/CPE sensor for trace detection of sulfamethoxazole (SMX) by modifying CPE with the as-prepared ZnO@ZIF-8 nano-composite. Compared with bare CPE, the oxidation peak current of the ZnO@ZIF-8/CPE sensor triggered by SMX increases significantly owing to the large specific surface area and high electron transfer rate of ZnO@ZIF-8. Under optimized conditions, the ZnO@ZIF-8/CPE sensor shows a wide linear range (0.04–50 μM) and low LOD (0.02 μM) for SMX. Additionally, this sensor exhibits good stability, selectivity, specificity and reproducibility. Thus, this sensor has been applied for electrochemical detection of SMX in eggs.

Table 5 Application of MOF/metallic oxide composites in electrochemical sensors

MOF composites	Target analysis	Linear range	Limit of detection (LOD)	References
UiO-66-NH <sub>2</sub> /TiO <sub>2</sub>	Chlorogenic acid	0.01–15 μM	7 nM	119
MIL-101(Fe)@Fe <sub>3</sub> O <sub>4</sub>	H <sub>2</sub> O <sub>2</sub>	0.005–0.02 mM	1.76 μM	120
Fe <sub>3</sub> O <sub>4</sub> @ZIF-8/RGO	Dopamine	0.002–10 μM	0.667 nM	121
ZnO@ZIF-8	Sulfamethoxazole	0.04–50 μM	0.02 μM	122
CuO/ZIF-8@NiF	Glucose	0.5–120 μM	0.1 μM	123
CuONPs/Ce-MOF	Glucose	5 nM–8.6 mM	2 nM	124



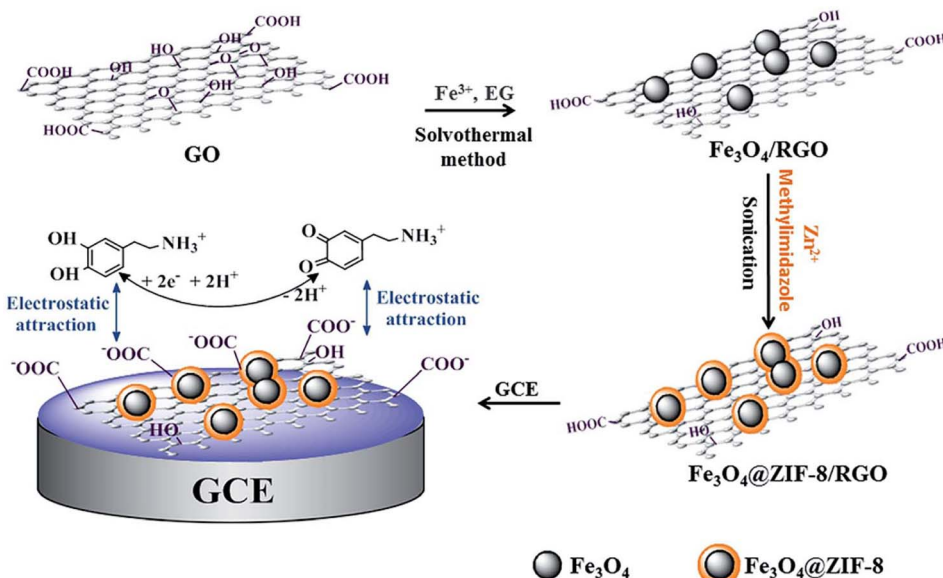


Fig. 12 Development of the  $\text{Fe}_3\text{O}_4@$ ZIF-8/RGO/GCE sensor and electrochemical detection of DA. Reprinted with permission from ref. 121. Copyright 2015 RSC Advances.

#### 4.3 MOF/CuO composite

As a key narrow-bandgap (1.2 eV) P-type semiconductor, CuO shows excellent physical and chemical properties. Hence, CuO has been widely applied in catalysis, sensing, and batteries.<sup>133–136</sup> Recently, CuO combined with MOF to construct MOF/CuO composite has been employed for developing enzyme-free glucose sensors, which can achieve highly sensitive detection.

Deng *et al.*<sup>123</sup> developed the CuO/ZIF-8@NiF electrochemical sensor for glucose detection by assembling CuO/ZIF-8 in Ni foam (NiF) (in pores and on surface). The presence of the CuO/ZIF-8@NiF composite increases surface area with a rise in electrochemical activity and enhances electron transfer efficiency. This sensor shows excellent electrocatalytic activity,

a wide linear range (0.5–120  $\mu\text{M}$ ), low LOD (0.1  $\mu\text{M}$ ), and high sensitivity ( $5640 \mu\text{A mM}^{-1} \text{cm}^{-2}$ ) for glucose. Additionally, the recovery rate of this sensor for glucose detection in human blood samples is 101.08–104.53%.

Zhang *et al.*<sup>124</sup> prepared the CuONPs/Ce-MOF composite *via* *in situ* adsorption of CuO on Ce-MOF, and developed the CuONPs/Ce-MOF/GCE electrochemical sensor by modifying GCE with the CuONPs/Ce-MOF composite for glucose detection (Fig. 14). The Cu(II) is oxidized to Cu(III) on the surface of the constructed sensor, and Cu(III) plays the role of catalyst, which can quickly oxidize glucose into gluconolactone and further produce glucose acid. Under optimized conditions, this sensor shows a good linearity (5 nM–8.6 mM) for glucose, with an LOD of 2 nM. Additionally, this sensor shows excellent selectivity,

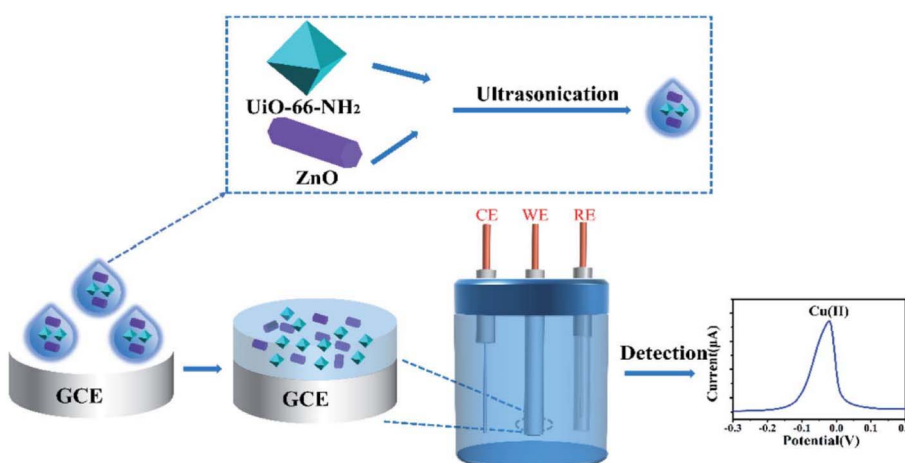


Fig. 13 Highly sensitive detection of  $\text{Cu}^{2+}$  at the  $\text{UiO-66-NH}_2/\text{ZnO}/\text{GCE}$  sensor. Reprinted with permission from ref. 132. Copyright 2022 RSC Advances.

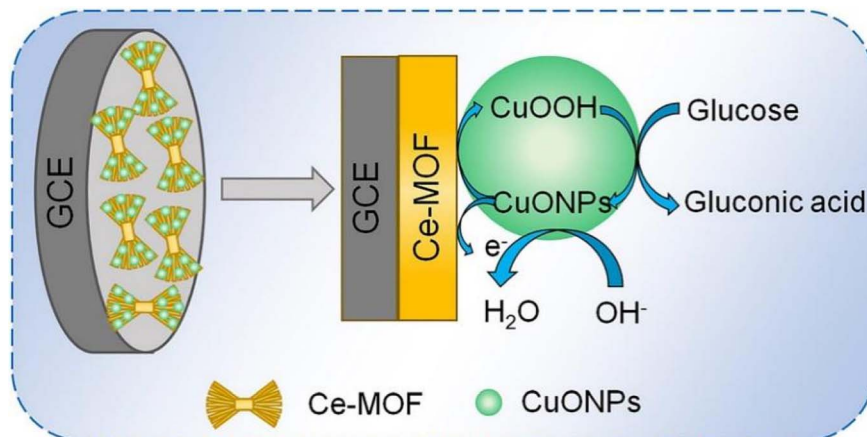


Fig. 14 Mechanism of glucose detection at the CuONPs/Ce-MOF/GCE sensor. Reprinted with permission from ref. 124. Copyright 2019 Ionics.

reproducibility, and stability, rendering it suitable for the accurate detection of glucose in human serum. Consequently, CuONPs/Ce-MOF/GCE is a promising non-enzymatic sensor for glucose.

## 5. Other MOF composites

Besides the MOF composites mentioned above, enzymes and polyoxometalates (POM) with excellent catalytic performance are combined with MOF to develop new functions that expand the application scope of MOF/enzyme and MOF/POM composites. Owing to their unique physical and chemical properties, these composites have been applied in various fields, especially electrochemical sensor.

### 5.1 MOF/enzyme composite

Enzymes are proteins with catalytic functions, and their catalytic efficiencies tend to be higher than those of conventional inorganic catalysts. Nevertheless, enzymes are hindered by their low stability, difficult recovery, easy denaturation and inactivation.<sup>137–139</sup> MOF as immobilized carrier can well protect

enzyme activity. Even in some unnatural environments (high temperature, organic solvent, *etc.*), MOF can also effectively prevent a large number of enzyme inactivation, so that the enzyme is easy to separate, efficient recovery and utilization, improving the life and efficiency of the enzyme.

Wang *et al.*<sup>140</sup> prepared the *Burkholderia cepacia* lipase (BCL) @MOF nano-fiber composite by using synthetic MOF fibers, and then developed an electrochemical biosensor by modifying GCE with the BCL@MOF nano-fiber using chitosan for detecting methyl parathion (MP) (Fig. 15). The developed BCL@MOF nano-fiber/chitosan/GCE sensor shows a wide linear range (0.1–38  $\mu$ M), low LOD (0.067  $\mu$ M), and high sensitivity for MP. Additionally, this sensor shows good reproducibility and stability. After storage for three weeks, the response of this sensor to MP exceeds 80% of the initial response. Additionally, this sensor has been used for accurate detection of MP in vegetables.

Song *et al.*<sup>141</sup> prepared the Cu-BTC MOF/3D-KSC electrode by growing the Cu-BTC MOF on a 3D macroporous carbon electrode (3D-KSC). Meanwhile, AuNPs were deposited on this electrode *via* electrodeposition, which was followed by

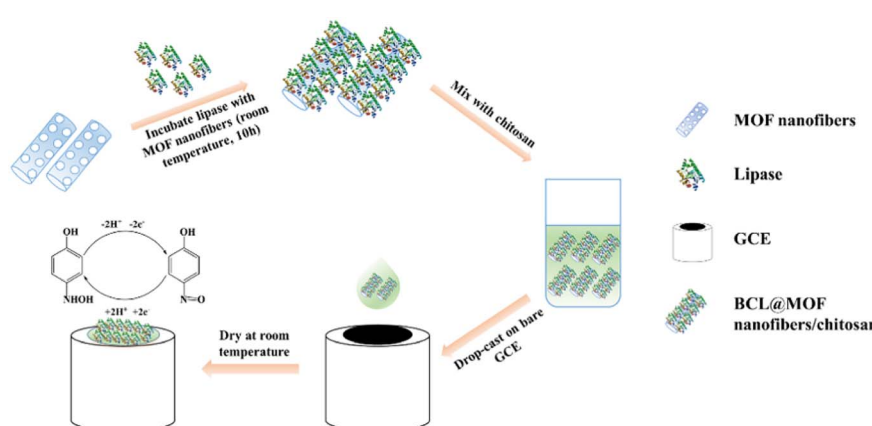


Fig. 15 Preparation of the BCL@MOF nanofibers/chitosan/GCE biosensor and sensitive detection of MP. Reprinted with permission from ref. 140. Copyright 2019 Talanta.



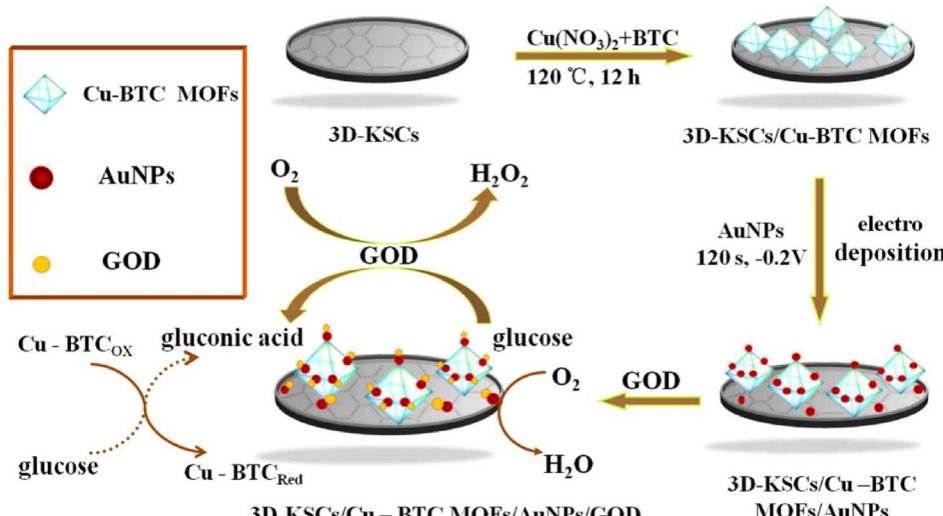


Fig. 16 Detection mechanism of glucose at 3D-KSCs/Cu-BTC MOF/AuNPs/GOD sensor. Reprinted with permission from ref. 141. Copyright 2018 Sensors and Actuators B: Chemical.

immobilization of glucose oxidase (GOD), to develop the 3D-KSCs/Cu-BTC MOF/AuNPs/GOD sensor (Fig. 16). The size of the prepared AuNPs was about 10–20 nm, which can not only fix GOD, but also improve the conductivity of Cu-BTC MOF. Due to the synergistic effect between Cu-BTC MOF and AuNPs, the prepared composite has high electrocatalytic activity, which can make glucose quickly produce gluconic acid. Under optimized experimental conditions, this sensor shows good linearity for glucose in the ranges of 0.0449–4.0 mM and 4.0–19.0 mM, while exhibiting an LOD of 14.77  $\mu$ M. Additionally, this sensor exhibits high selectivity and good reproducibility for glucose detection in serum. Overall, this sensor provides a reliable and accurate approach for glucose detection.

## 5.2 MOF/POM composite

POM is a metal–oxygen cluster compound with a cage structure. Typically, POM exhibits unique electrochemical redox activity and can participate in fast and reversible multi-electron transfer reactions. Consequently, POM has been regarded as a promising electrocatalytic material.<sup>142,143</sup> Composites prepared by encapsulating POM into MOF are characterized by their large specific surface area, high chemical stability, and easy reusability.<sup>144,145</sup>

Fernandes *et al.*<sup>146</sup> prepared a novel hybrid composite  $\text{PMo}_{10}\text{V}_2@\text{MIL-101}$  by encapsulating tetra-butyl ammonium (TBA) of  $[\text{PMo}_{10}\text{V}_2\text{O}_{40}]^{5-}$  ( $\text{PMo}_{10}\text{V}_2$ ) into MIL-101(Cr), after which they developed an effective electrochemical sensor by modifying a graphite electrode (PG) with  $\text{PMo}_{10}\text{V}_2@\text{MIL-101}$ . Owing to the large specific surface area and unique pore structure of MIL-101, as well as the excellent electrochemical activity of  $\text{PMo}_{10}\text{V}_2$ , this sensor exhibits good electrochemical responses for both individual and simultaneous detection of AA and DA. Furthermore, combining MIL-101(Cr),  $\text{PMo}_{10}\text{V}_2$ , and PG is characterized by facile preparation and low cost.

Zhang *et al.*<sup>147</sup> prepared the POMOF/rGO composite by using a one-pot process, and developed the POMOF/rGO/GCE

electrochemical sensor by modifying GCE using the POMOF/rGO/GCE for detecting DA. POMOF has open channels and rich metal centers, which can be used as catalytic active sites. RGO exhibits large surface area, which can promote electron transfer in the composite. This unique structure can adsorb DA molecules by interacting with the  $\pi-\pi$  bond of graphene, so that POMOF/rGO/GCE sensor has better catalytic activity for DA. The proposed sensor has a wide linear range (1–200  $\mu$ M) and a low detection limit (80.4 nM). Additionally, the developed electrochemical sensor shows good stability, high selectivity, and high interference resistance. As a non-noble metal catalyst, the as-prepared POMOF/rGO composite shows great application potential for DA detection, thereby facilitating the advances in POM sensors.

## 6. Conclusions and outlook

Due to their structural diversity, good conductivity and biocompatibility of MOF composites, made their wide applications in the detection of metal ions, organic pollutants, pesticides, and key biomolecules (*e.g.*, glucose, DA, UA,  $\text{H}_2\text{O}_2$ , AA). Compared with traditional detection methods, the electrochemical detection method has the advantages of fast analysis speed, low detection cost and easy miniaturization. Excellent structural characteristics and large membrane surface area of MOF composites provide recognition space for the detection of target molecules. In addition, adjusting the pore size of the corresponding MOF for different target objects also significantly improves the recognition ability and specific selectivity of the fabricated sensor for target molecules.

At present, MOF composites sensors have made some progress in laboratory and some practical samples. For example, researchers synthesized Co-MOF by one-step method, which has a good catalytic effect on the electrooxidation of hydrazine and the electroreduction of nitrobenzene, and realized the detection of these two substances.  $\text{Au-SH-SiO}_2@\text{Cu}$

MOF composite was prepared for determination of L-cysteine by electrocatalytic oxidation of cysteine. Through solvothermal synthesis of Cu(tpa)-GO-MOF material, an electrochemical sensor for the detection of dopamine and acetaminophen was fabricated. However, some issues need to be solved before these sensors can be used commercially at a large scale. First, MOF materials tend to have low structural stability and low conductivity, while catalytic active sites in these composites can barely bind to the reactants in a rapid manner; this results in poor detection of the target molecules by the developed sensors. Second, although composites on the sensor are readily exposed to decomposition in water or under UV radiation, functional materials can enhance the conductivity of MOF under such conditions. Consequently, development of MOF composites with high stability, conductivity, and electrochemical response remains a challenge. Third, despite excellent electrochemical detection, previously reported MOF composites are limited by high costs, complicated synthesis processes, and absence of large-scale production. Finally, sensors based on MOF/enzyme composites are not ready for practical applications owing to complicated production processes, high production requirements, and difficult characterization; however, these composites can be used to detect specific chemical species.

The combination of MOF and functional materials equips the MOF composites with diversified functional groups, good conductivity, and abundant active sites; thus, these composites exhibit suitable physical and electrochemical performances for electrochemical sensor. Despite the great potential of MOF composites in electrochemical sensor, large-scale production of non-toxic and environmentally-friendly sensors for real-world detections requires more efforts. The following conclusions have been established in the review:

(1) To realize the large-scale application of MOF composites, it is necessary to find cost effective yet highly active metal particles that can replace noble metals used in existing MOF composites.

(2) To enhance the water stability of MOF composites and reduce the influences of other solvent molecules on coordination centers, a green route for synthesizing MOF composites in aqueous solutions should be developed.

(3) Although MOF materials can be used for immobilization and encapsulation of enzymes, the preparation method of microporous MOF that is suitable for enzyme loading and corresponding production processes requires further optimization.

(4) MOF composites can be combined with nano-fiber paper, portable fluorescence detector, paper chip technology, and smart phones to develop facile, rapid, accurate, and portable electrochemical sensing methods.

## List of acronyms and abbreviations

MOF	Metal-organic frameworks
MNPs	Metallic nanoparticles
AuNPs	Au nanoparticles
SWNTs	Single-walled carbon nanotubes

LOD	Limit of detection
CNT	Carbon nanotube
GCE	Glassy carbon electrode
MWCNTs	Multi-walled carbon nanotubes
PBS	Phosphate buffered solution
DPV	differential pulse voltammetry
GN	Graphene
PAMAM	Polyamidoamine
ERGO	Electrochemically reduced graphene oxide
1-OHPyr	1-Hydroxy pyrene
Fe <sub>3</sub> O <sub>4</sub> -GO	Fe <sub>3</sub> O <sub>4</sub> -graphene oxide
ZEA	Zearanene
DFT	Density functional theory
AuNPs	Au nanoparticles
N-GQDs	N-Doped graphene quantum dots
PVP	Polyvinylpyrrolidone
PVP-rGO	Dispersed reduced graphene oxide
SAL	Salbutamol
PDA	Polydopamine
MTZ	Metronidazole
CPE	Carbon-pasted electrode
PtNPs	Pt nanoparticles
TDZ	Tinidazole
LOD	Limit of detection
SMX	Sulfamethoxazole
NiF	Ni foam
POM	Polyoxometalates
BCL	Burkholderia cepacia lipase
MP	Methyl parathion
3D-KSC	3D macroporous carbon electrode
GOD	Glucose oxidase
TBA	Tetra-butyl ammonium
PG	Graphite electrode
ZIF	Zeolitic imidazolate framework
BTC	1,3,5-Benzenetricarboxylic acid

## Author contribution

Wanqing Zhang and Kang Hua: conception or design and data collection. Xijiao Li and Xiaoman Ding: project administration and writing original draft. Aili Sun, Xinxin Hu and Ziwei Nie: literature survey, drafting and resources. Yongsheng Zhang and Jichao Wang: writing-review and editing. Renlong Li and Shanqin Liu: software, critical revision and investigation.

## Conflicts of interest

The authors declare no competing interests.

## Acknowledgements

This work was financially supported by the National Natural Science Foundation of China (No. 51802082, No. 51903073), Key Scientific and Technological Project of Henan Province (No. 232102230028 and 222102320100), Program for Science & Technology Innovation Talents in Universities of Henan Province (No. 21HATIT016), Key Project of Science and Technology



Program of Xinxiang City (No. GG2021005 and 21ZD005) and National College Student Innovation and Entrepreneurship Training (No. 202110467024).

## References

- 1 C. H. Chuang and C. W. Kung, *Electroanal.*, 2020, **32**, 1885–1895.
- 2 V. N. Palakollu, D. Chen, J. N. Tang, L. Wang and C. Liu, *Microchim. Acta*, 2022, **189**, 161.
- 3 S. Wang, T. Zhang, X. Zhu, S. Zu, Z. Xie, X. Lu, M. Zhang, L. Song and Y. Jin, *Molecules*, 2022, **27**, 4571.
- 4 H. Y. Li, S. N. Zhao, S. Q. Zang and J. Li, *Chem. Soc. Rev.*, 2020, **49**, 6364–6401.
- 5 S. Wang, W. Xie, P. Wu, G. Lin, Y. Cui, J. Tao, G. Zeng, Y. Deng and H. Qiu, *Nat. Commun.*, 2022, **13**, 6673.
- 6 X. Xiao, L. Zou, H. Pang and Q. Xu, *Chem. Soc. Rev.*, 2020, **49**, 301–331.
- 7 Y. Dou, C. Grande, A. Kaiser and W. Zhang, *Sci. China Mater.*, 2021, **64**, 1742–1750.
- 8 R. Colorado-Peralta, J. María Rivera-Villanueva, J. Manuel Mora-Hernández, D. Morales-Morales and L. Ángel Alfonso-Herrera, *Polyhedron*, 2022, **224**, 115995.
- 9 H. Li, L. Shi, C. Li, X. Fu, Q. Huang and B. Zhang, *ACS Appl. Mater. Interfaces*, 2020, **12**, 34095–34104.
- 10 J. Zhang, B. An, Y. Cao, Z. Li, J. Chen, X. He and C. Wang, *ACS Appl. Energy Mater.*, 2021, **4**, 13567–13574.
- 11 A. Ahmad, S. Khan, S. Tariq, R. Luque and F. Verpoort, *Mater. Today*, 2022, **55**, 137–169.
- 12 X. Peng, L. Chen and Y. Li, *Mol. Catal.*, 2022, **529**, 112568.
- 13 M. Le, Q. L. Ni, L. H. Zeng, C. Y. Yuan, X. J. Wang, S. M. Li and L. C. Gui, *Mol. Catal.*, 2022, **533**, 112786.
- 14 A. K. Thakur, M. Majumder, S. P. Patole, K. Zaghib and M. V. Reddy, *Mater. Adv.*, 2021, **2**, 2457–2482.
- 15 Y. Zheng, S. S. Zheng, H. G. Xue and H. Pang, *J. Mater. Chem. A*, 2019, **7**, 3469–3491.
- 16 H. M. Shen, *Coord. Chem. Rev.*, 2022, **470**, 214715.
- 17 V. Shrivastav, S. Sundriyal, P. Goel, H. Kaur, S. K. Tuteja, K. Vikrant, K. H. Kim, U. K. Tiwari and A. Deep, *Coord. Chem. Rev.*, 2019, **393**, 48–78.
- 18 M. Attia, R. D. Glickman, G. Romero, B. Chen, A. J. Brenner and J. Y. Ye, *J. Drug Delivery Sci. Technol.*, 2022, **76**, 103770.
- 19 P. Markopoulou, N. Panagiotou, A. Li, R. Bueno-Perez, D. Madden, S. Buchanan, D. Fairen-Jimenez, P. G. Shiels and R. S. Forgan, *Cell Rep. Phys. Sci.*, 2020, **1**, 100254.
- 20 L. Q. Wei, J. Y. Lu, Q. Q. Li, Y. Zhou, L. L. Tang and F. Y. Li, *Inorg. Chem. Commun.*, 2017, **78**, 43–47.
- 21 M. Yang, Z. Sun, H. Jin and R. Gui, *Microchem. J.*, 2022, **177**, 107319.
- 22 D. Zhang, J. Wang, Q. Wang, S. Huang, H. Feng and H. Luo, *J. Energy Storage*, 2019, **25**, 100904.
- 23 Y. Li, B. Huang, X. Zhao, Z. Luo, S. Liang, H. Qin and L. Chen, *J. Power Sources*, 2022, **527**, 231149.
- 24 M. A. Tahir, N. Arshad and M. Akram, *J. Energy Storage*, 2022, **47**, 103530.
- 25 S. Shin and M. W. Shin, *Appl. Surf. Sci.*, 2021, **540**, 148295.
- 26 H. Huang, Y. Chen, Z. Chen, J. Chen, Y. Hu and J. J. Zhu, *J. Hazard. Mater.*, 2021, **416**, 125895.
- 27 Y. Hu, C. Wang, P. Zhao, L. Zhang, J. Fei and Y. Xie, *Talanta*, 2022, **246**, 123520.
- 28 D. Duan, H. Yang, Y. Ding, L. Li and G. Ma, *Electrochim. Acta*, 2019, **302**, 137–144.
- 29 E. Saeb and K. Asadpour-Zeynali, *Microchem. J.*, 2022, **172**, 106976.
- 30 F. Fallah, M. R. Shishehbore and A. Sheibani, *Talanta*, 2023, **252**, 123776.
- 31 W. Li, L. Xu, X. Zhang, Z. Ding, X. Xu, X. Cai, Y. Wang, C. Li and D. Sun, *Sens. Actuators, B*, 2023, **378**, 133153.
- 32 Q. Zhou, L. Yang, Z. Kan, J. Lyu, M. X. Wang, B. Dong, X. Bai, Z. Chang, H. Song and L. Xu, *Chem. Eng. J.*, 2022, **450**, 138014.
- 33 M. Ma, X. Lu, Y. Guo, L. Wang and X. Liang, *TrAC, Trends Anal. Chem.*, 2022, **157**, 116741.
- 34 T. Du, J. Wang, L. Zhang, S. Wang, C. Yang, L. Xie, Z. Liu, Y. Ni, X. Xie, J. Sun, W. Zhang and J. Wang, *Chem. Eng. J.*, 2022, **431**, 134050.
- 35 G. R. Xu, Z. H. An, K. Xu, Q. Liu, R. Das and H. L. Zhao, *Chem. Eng. J.*, 2021, **427**, 213554.
- 36 J. Cui, X. Xu, C. Yang, J. Wang, Q. Guo and G. Nie, *Sens. Actuators, B*, 2023, **378**, 133141.
- 37 J. Zhao, Y. N. Wang, W. W. Dong, Y. P. Wu, D. S. Li and Q. C. Zhang, *Inorg. Chem.*, 2016, **55**, 3265–3271.
- 38 J. Ye, L. Zhao, R. F. Bogale, Y. Gao, X. Wang, X. Qian, S. Guo, J. Zhao and G. Ning, *Chem.-Eur. J.*, 2015, **21**, 2029–2037.
- 39 S. Rani, B. Sharma, R. Malhotra, S. Kumar, R. S. Varma and N. Dilbaghi, *Environ. Res.*, 2020, **191**, 110005.
- 40 Y. Cao, L. Wang, C. Shen, C. Wang, X. Hu and G. Wang, *Sens. Actuators, B*, 2019, **283**, 487–494.
- 41 J. Song, M. Huang, X. Lin, S. F. Y. Li, N. Jiang, Y. Liu, H. Guo and Y. Li, *Chem. Eng. J.*, 2022, **427**, 130913.
- 42 G. Li, S. Liu, D. Liu and N. Zhang, *Inorg. Chem. Commun.*, 2021, **130**, 108713.
- 43 Y. Lu, Z. Wang, X. Mu, Y. Liu, Z. Shi, Y. Zheng and W. Huang, *Microchem. J.*, 2022, **175**, 107131.
- 44 S. Xie, J. Ye, Y. Yuan, Y. Chai and R. Yuan, *Nanoscale*, 2015, **7**, 18232–18238.
- 45 Q. Wang, S. Cheng, S. Ren and Z. Zheng, *Microchem. J.*, 2022, **183**, 107963.
- 46 K. Z. Mousaabadi, A. A. Ensafi and B. Rezaei, *Chemosphere*, 2022, **303**, 135149.
- 47 N. M. Umesh, J. Antolin Jesila, S. F. Wang, N. Vishnu and Y. J. Yang, *Microchem. J.*, 2021, **160**, 105747.
- 48 G. A. Bodkhe, B. S. Hedau, M. A. Deshmukh, H. K. Patil, S. M. Shirsat, D. M. Phase, K. K. Pandey and M. D. Shirsat, *J. Mater. Sci.*, 2020, **56**, 474–487.
- 49 J. Tang, S. Jiang, Y. Liu, S. Zheng, L. Bai, J. Guo and J. Wang, *Mikrochim. Acta*, 2018, **185**, 486.
- 50 Y. Li, W. Ye, Y. Cui, B. Li, Y. Yang and G. Qian, *J. Mol. Struct.*, 2020, **1209**, 127986.
- 51 G. Wang, M. Yu and X. Feng, *Chem. Soc. Rev.*, 2021, **50**, 2388–2443.
- 52 W. X. Dong, Y. F. Qu, X. Liu and L. F. Chen, *FlatChem*, 2023, **37**, 100467.



53 Y. Wu, Y. Wei and Y. Ji, *Giant*, 2023, **13**, 100136.

54 S. K. Singh, P. Azad, M. J. Akhtar and K. K. Kar, *ACS Appl. Nano Mater.*, 2018, **1**, 4746–4755.

55 F. Cai, Q. Wang, X. Chen, W. Qiu, F. Zhan, F. Gao and Q. Wang, *Biosens. Bioelectron.*, 2017, **98**, 310–316.

56 M. Hadi, M. Bayat, H. Mostaanzadeh, A. Ehsani and A. Yeganeh-Faal, *Int. J. Environ. Anal. Chem.*, 2018, **98**, 197–214.

57 W. Bai, S. Li, J. Ma, W. Cao and J. Zheng, *J. Mater. Chem. A*, 2019, **7**, 9086–9098.

58 Y. Y. Zheng, C. X. Li, X. T. Ding, Q. Yang, Y. M. Qi, H. M. Zhang and L. T. Qu, *Chin. Chem. Lett.*, 2017, **28**, 1473–1478.

59 M. Saraf, R. Rajak and S. M. Mobin, *J. Mater. Chem. A*, 2016, **4**, 16432–16445.

60 X. Wang, J. Zhang, Y. Wei, T. Xing, T. Cao, S. Wu and F. Zhu, *Analyst*, 2020, **145**, 1933–1942.

61 F. Wang, X. Chen, L. Chen, J. Yang and Q. Wang, *Mater. Sci. Eng., C*, 2019, **96**, 41–50.

62 M. Hadi, H. Poorgholi, H. Mostaanzadeh and S. Afr, *J. Chem.*, 2016, **69**, 132–139.

63 W. Q. Zhang, Z. Y. Zhang, Y. C. Li, J. Chen, X. B. Li, Y. D. Zhang and Y. P. Zhang, *Sens. Actuators, B*, 2017, **247**, 756–764.

64 D. Li, X. Qiu, H. Guo, D. Duan, W. Zhang, J. Wang, J. Ma, Y. Ding and Z. Zhang, *Environ. Res.*, 2021, **202**, 111605.

65 B. Dai, R. Zhou, J. Ping, Y. Ying and L. Xie, *TrAC, Trends Anal. Chem.*, 2022, **154**, 116658.

66 S. Gulati, B. H. Lingam, S. Kumar, K. Goyal, A. Arora and R. S. Varma, *Chemosphere*, 2022, **299**, 134468.

67 H. Gharaei, A. Nikfarjam, F. Saniei and A. Abbasi, *Microsyst. Technol.*, 2016, **23**, 2797–2805.

68 L. R. Pokhrel, N. Ettore, Z. L. Jacobs, A. Zarr, M. H. Weir, P. R. Scheuerman, S. R. Kanel and B. Dubey, *Sci. Total Environ.*, 2017, **574**, 1379–1388.

69 D. Qin, T. Li, X. Li, J. Feng, T. Tang and H. Cheng, *Anal. Methods*, 2021, **13**, 5450–5457.

70 M. Ikram, M. A. Bari, M. Bilal, F. Jamal, W. Nabgan, J. Haider, A. Haider, G. Nazir, A. D. Khan, K. Khan, A. K. Tareen, Q. Khan, G. Ali, M. Imran, E. Caffrey and M. Maqbool, *Biomater. Adv.*, 2022, **145**, 213234.

71 S. R. Benjamin and E. J. Miranda Ribeiro Júnior, *Curr. Opin. Environ. Sci. Health*, 2022, **29**, 100381.

72 R. Ghosh, M. Aslam and H. Kalita, *Mater. Today Commun.*, 2022, **30**, 103182.

73 M. Hernaez, *Sensors*, 2020, **20**, 3196.

74 X. Hou, H. Xu, T. Zhen and W. Wu, *Trends Food Sci. Technol.*, 2020, **105**, 76–92.

75 J. Li, J. Xia, F. Zhang, Z. Wang and Q. Liu, *Talanta*, 2018, **181**, 80–86.

76 H. Cui, S. Cui, Q. Tian, S. Zhang, M. Wang, P. Zhang, Y. Liu, J. Zhang and X. Li, *ACS Omega*, 2021, **6**, 31184–31195.

77 Y. Zeng, M. B. Camarada, X. Lu, K. Tang, W. Li, D. Qiu, Y. Wen, G. Wu, Q. Luo and L. Bai, *Food Chem.*, 2022, **370**, 131024.

78 M. F. R. Hanifah, J. Jaafar, M. Aziz, M. H. D. Othman, A. F. Ismail, M. A. Rahman, S. N. Wan Ikhwan, G. Ur Rehman, A. Z. Abdul Ajid and S. Z. Salleh, *Mater. Today: Proc.*, 2021, **46**, 1889–1894.

79 S. T. Renjie Qu, J. Zhang and L. Wu, *ACS Sustainable Chem. Eng.*, 2018, **6**, 15560–15569.

80 W. Zhang, J. Chen, Y. Li, W. Yang, Y. Zhang and Y. Zhang, *RSC Adv.*, 2017, **7**, 5628–5635.

81 M. Jouyandeh, S. M. Sajadi, F. Seidi, S. Habibzadeh, M. T. Munir, O. Abida, S. Ahmadi, D. Kowalkowska-Zedler, N. Rabiee, M. Rabiee, G. Heidari, M. Hassanpour, E. Nazarzadeh Zare and M. R. Saeb, *OpenNano*, 2022, **8**, 100104.

82 X. Wang, Y. Wang and Y. Ying, *TrAC, Trends Anal. Chem.*, 2021, **143**, 116395.

83 M. Nemiwal, M. Sillanpää, F. Banat and D. Kumar, *Inorg. Chem. Commun.*, 2022, **143**, 109739.

84 Y. Liu, Z. Liu, D. Huang, M. Cheng, G. Zeng, C. Lai, C. Zhang, C. Zhou, W. Wang, D. Jiang, H. Wang and B. Shao, *Coord. Chem. Rev.*, 2019, **388**, 63–78.

85 P. Falcaroa, R. Riccoa, A. Yazdib, I. Imazb, S. Furukawac, D. Maspoch, R. Ameloot, J. D. Evans and C. J. Doonan, *Coord. Chem. Rev.*, 2016, **307**, 237–254.

86 D. K. Yadav, V. Ganesan, P. K. Sonkar, R. Gupta and P. K. Rastogi, *Electrochim. Acta*, 2016, **200**, 276–282.

87 D. K. Yadav, V. Ganesan, F. Marken, R. Gupta and P. K. Sonkar, *Electrochim. Acta*, 2016, **219**, 482–491.

88 W. Meng, Y. Wen, L. Dai, Z. He and L. Wang, *Sens. Actuators, B*, 2018, **260**, 852–860.

89 L. Zhang, S. Li, J. Xin, H. Ma, H. Pang, L. Tan and X. Wang, *Microchim. Acta*, 2018, **186**, 9.

90 J. Yang, L. Yang, H. Ye, F. Zhao and B. Zeng, *Electrochim. Acta*, 2016, **219**, 647–654.

91 H. Chen, T. Yang, F. Liu and W. Li, *Sens. Actuators, B*, 2019, **286**, 401–407.

92 M. Deng, X. Bo and L. Guo, *J. Electroanal. Chem.*, 2018, **815**, 198–209.

93 L. Shi, X. Zhu, T. Liu, H. Zhao and M. Lan, *Sens. Actuators, B*, 2016, **227**, 583–590.

94 C. Yuan, B. Qiu, M. T. Sun, W. J. Hu, H. Tan and S. H. Wang, *Appl. Surf. Sci.*, 2022, **614**, 156234.

95 A. Corma and H. Garcia, *Chem. Soc. Rev.*, 2008, **37**, 2096–2126.

96 M. Hegde, P. Pai, M. G. Shetty and K. S. Babitha, *Environ. Nanotechnol. Monit. Manage.*, 2022, **18**, 100756.

97 R. Sun, R. Lv, Y. Li, T. Du, L. Chen, Y. Zhang, X. Zhang, L. Zhang, H. Ma, H. Sun and Y. Qi, *Food Control*, 2023, **145**, 109491.

98 B. Hatamluyi, M. Rezayi, H. R. Beheshti and M. T. Boroushaki, *Sens. Actuators, B*, 2020, **318**, 128219.

99 W. Dang, Y. Sun, H. Jiao, L. Xu and M. Lin, *J. Electroanal. Chem.*, 2020, **856**, 113592.

100 S. H. Sun, R. C. Zhao, W. W. Hao, H. M. Guo, L. Shi and X. O. Su, *Russ. J. Electrochem.*, 2019, **55**, 908–919.

101 Z. Lotfi, M. B. Gholivand, M. Shamsipur and M. mirzaei, *Sens. Actuators, B*, 2022, **903**, 163912.

102 A. Shahzad, W. S. Kim and T. Yu, *RSC Adv.*, 2015, **5**, 28652–28661.



103 S. Wang, M. Wang, C. Li, H. Li, C. Ge, X. Zhang and Y. Jin, *Sens. Actuators, B*, 2020, **311**, 127919.

104 S. Rong, L. Zou, Y. Zhu, Z. Zhang, H. Liu, Y. Zhang, H. Zhang, H. Gao, H. Guan, J. Dong, Y. Guo, F. Liu, X. Li, H. Pan and D. Chang, *Microchem. J.*, 2021, **168**, 106410.

105 G. A. Bodkhe, D. D. Khandagale, M. S. More, M. A. Deshmukh, N. N. Ingle, P. W. Sayyad, M. M. Mahadik, S. M. Shirsat, M. S. Al-Buriahi, M. L. Tsai, M. Kim and M. D. Shirsat, *Ceram. Int.*, 2022, **4**, 6772–6779.

106 J. Tang, T. Hu, N. Li, Y. Zhu, J. Li, S. Zheng and J. Guo, *Microchem. J.*, 2022, **179**, 107461.

107 Y. Dong, C. Duan, Q. Sheng and J. Zheng, *Analyst*, 2019, **144**, 521–529.

108 J. Fan, H. Wang, X. Zeng, L. Su and X. Zhang, *J. Electroanal. Chem.*, 2022, **914**, 116323.

109 H. Saedi, M. R. Fat'hi and B. Zargar, *J. Chin. Chem. Soc.*, 2021, **68**, 1954–1964.

110 J. Chen, C. Yu, Y. Zhao, Y. Niu, L. Zhang, Y. Yu, J. Wu and J. He, *Biosens. Bioelectron.*, 2017, **91**, 892–899.

111 J. Ru, X. Wang, Z. Zhou, J. Zhao, J. Yang, X. Du and X. Lu, *Anal. Chim. Acta*, 2022, **1195**, 339451.

112 Y. Yang, Z. Yang, J. Lv, R. Yuan and Y. Chai, *Talanta*, 2017, **169**, 44–49.

113 L. Chen, Z. Liu, Z. Guo and X. J. Huang, *J. Mater. Chem. A*, 2020, **8**, 17326–17359.

114 Y. Zhu, Q. Lin, Y. Zhong, H. A. Tahini, Z. Shao and H. Wang, *Energy Environ. Sci.*, 2020, **13**, 3361–3392.

115 L. Wang, C. Shi, L. Wang, L. Pan, X. Zhang and J. J. Zou, *Nanoscale*, 2020, **12**, 4790–4815.

116 P. Dharmalingam, G. Palani, R. Apsari, K. Kannan, S. K. Lakkaboyana, K. Venkateswarlu, V. Kumar and Y. Ali, *Mater. Today Sustain.*, 2022, **20**, 100232.

117 Y. Sun, Z. Zhao, K. Suematsu, P. Li, W. Zhang and J. Hu, *Mater. Res. Bull.*, 2022, **146**, 111607.

118 X. Ren, Z. Xu, D. Liu, Y. Li, Z. Zhang and Z. Tang, *Sens. Actuators, B*, 2022, **357**, 131384.

119 Y. Wang, H. Chen, X. Hu and H. Yu, *Analyst*, 2016, **141**, 4647–4653.

120 F. Salman, A. Zengin and H. Çelik Kazici, *Ionics*, 2020, **26**, 5221–5232.

121 Y. Wang, Y. Zhang, C. Hou and M. Liu, *RSC Adv.*, 2015, **5**, 98260–98268.

122 S. Guo, *Int. J. Electrochem. Sci.*, 2021, **16**, 210950.

123 L. Deng, S. Fan, Y. Chen, J. Chen, Z. Mai and Z. Xiao, *Ind. Eng. Chem. Res.*, 2022, **61**, 7312–7321.

124 J. Zhang, L. Chen and K. Yang, *Ionics*, 2019, **25**, 4447–4457.

125 J. Zhang, X. Tian, X. Cui, A. Zheng, J. Li, Y. Bai and Y. Zheng, *Talanta*, 2023, **252**, 123895.

126 A. N. Egler-Kemmerer, A. Baki, N. Löwa, O. Kosch, R. Thiermann, F. Wiekhorst and R. Bleul, *J. Magn. Magn. Mater.*, 2022, **564**, 169984.

127 T. A. P. Rocha-Santos, *TrAC, Trends Anal. Chem.*, 2014, **62**, 28–36.

128 Y. Y. Chang, *Detection of oxytetracycline in food by magnetic MOF surface molecularly imprinted electrochemical sensor*, Shanxi University, Shanxi, 2020.

129 S. Ananthi, M. Kavitha, E. Ranjith Kumar, T. Prakash, R. Vandamar Poonguzhali, B. Ranjithkumar, A. Balamurugan, C. Srinivas and D. L. Sastry, *Inorg. Chem. Commun.*, 2022, **146**, 110152.

130 K. O. Olumurewa and M. A. Eleruja, *Phys. B: Condens. Matter*, 2023, **650**, 414588.

131 J. Zhang, X. Jia, T. Liu, J. Yang, S. Wang, Y. Li, D. Shao, L. Feng and H. Song, *Ceram. Int.*, 2022, **4**, 5861–5871.

132 Z. Li, Q. Li, R. Jiang, Y. Qin, Y. Luo, J. Li, W. Kong, Z. Yang, C. Huang, X. Qu, T. Wang, L. Cui, G. Wang, S. Yang, Z. Liu and X. Guo, *RSC Adv.*, 2022, **12**, 5062–5071.

133 F. Bayansal and H. A. Çetinkara, *J. Alloys Compd.*, 2022, **926**, 166737.

134 F. Guo, C. Feng, Z. Zhang, L. Zhang, C. Xu, C. Zhang, S. Lin, H. Wu, B. Zhang, A. Tabusi and Y. Huang, *Sens. Actuators, B*, 2023, **375**, 132885.

135 C. Feng, C. Zhang, C. Xu, S. Lin, B. Zhang, H. Wu, Z. Zhang, X. Guo, H. Bai and F. Guo, *Sens. Actuators, B*, 2023, **374**, 132827.

136 F. Guo, C. Feng, Z. Zhang, H. Wu, C. Zhang, X. Feng, S. Lin, C. Xu, B. Zhang and H. Bai, *Sens. Actuators, B*, 2022, **364**, 131898.

137 Y. Du, X. Jia, L. Zhong, Y. Jiao, Z. Zhang, Z. Wang, Y. Feng, M. Bilal, J. Cui and S. Jia, *Coord. Chem. Rev.*, 2022, **454**, 214327.

138 S. Xu, X. Qi, S. Gao, Y. Zhang, H. Wang, Y. Liang, F. Kong, R. Wang, Y. Wang, S. Yang and Y. An, *Enzyme Microb. Technol.*, 2023, **162**, 110134.

139 J. Liu, J. Liang, J. Xue and K. Liang, *Small*, 2021, **17**, 2100300.

140 Z. Wang, B. Ma, C. Shen and L. Z. Cheong, *Talanta*, 2019, **197**, 356–362.

141 Y. Song, M. Xu, C. Gong, Y. Shen, L. Wang, Y. Xie and L. Wang, *Sens. Actuators, B*, 2018, **257**, 792–799.

142 Q. Zhang, J. Ondus, J. Mills, A. Bahadori, J. Smith, T. Jordan, H. Xu and S. J. Hwu, *J. Solid State Chem.*, 2020, **287**, 121368.

143 Y. Zhang, Y. Zhang, L. Li, J. Chen, P. Li and W. Huang, *J. Electroanal. Chem.*, 2020, **861**, 113939.

144 Q. Liu, H. Lin, J. Lu, Y. Zhang and X. Wang, *J. Solid State Chem.*, 2022, **308**, 122911.

145 L. Tan, D. Guo, J. Liu, X. Song, Q. Liu, R. Chen and J. Wang, *J. Electroanal. Chem.*, 2019, **836**, 112–117.

146 D. M. Fernandes, A. D. Barbosa, J. Pires, S. S. Balula, L. Cunha-Silva and C. Freire, *ACS Appl. Mater. Interfaces*, 2013, **5**, 13382–13390.

147 W. Zhang, G. Jia, Z. Li, C. Yuan, Y. Bai and D. Fu, *Adv. Mater. Interfaces*, 2017, **4**, 1601241.

